

**THE DISTRIBUTION OF SEROTONINERGIC AND
NORADRENERGIC SYNAPSES ON THE DENDRITIC TREES OF
SPINAL MOTONEURONS**

by

STEVEN JAMES MONTAGUE

A thesis submitted to the Centre for Neuroscience

In conformity with the requirements for

the degree of Master of Science

Queen's University

Kingston, Ontario, Canada

(September, 2008)

Copyright © Steven James Montague, 2008

Abstract

The currents generated by excitatory and inhibitory synapses on motoneurons can be amplified by noradrenalin and serotonin. Both of these neurotransmitters act, and interact, via the same G_q -protein second-messenger system to modulate L-type Ca^{++} , persistent- Na^+ , and leak K^+ channels on motoneuron dendrites. However, noradrenergic and serotonergic synapses only modulate nearby excitatory and inhibitory synapses, so their relative distributions play a major role in the regulation of the overall output of the motoneuron. Moreover, the relative proximity between noradrenergic and serotonergic synapses may allow their individual effects to combine nonlinearly when co-activated, thereby regulating the magnitude of the amplification. The goal of the present study is to determine whether the distributions of noradrenergic and serotonergic synapses are biased along motoneuron dendritic trees.

The dendritic trees of five intracellularly stained feline splenius motoneurons were reconstructed. On them were plotted the locations of noradrenergic and serotonergic contacts, as determined by immunohistochemistry. The distribution of noradrenergic contacts was moderately biased both dorsally and distally in all five cells. Serotonergic contacts on the same neurons showed a moderate ventral bias. These findings suggest that excitatory and inhibitory inputs located dorsally and/or distally are preferentially amplified by noradrenergic synapses. Also, those synapses which are located ventrally are favorably amplified by serotonergic synapses. Both serotonergic and noradrenergic contacts are strongly biased towards innervation along small diameter ($<2\mu\text{m}$) dendrites.

The relative distributions between serotonergic and noradrenergic contacts have also been analyzed for all five cells. There was a bias towards minimizing the distance between like contacts (NE to NE and 5-HT to 5-HT). This increases the likelihood of interaction within populations when contacts are co-activated. Conversely, the distances between neighbouring noradrenergic and serotonergic contacts (NE to 5-HT and 5-HT to NE) were biased towards greater separation. This decreases the likelihood of interaction between populations when contacts are co-activated.

In summary, these findings suggest that noradrenalin and serotonin, having different location biases along the dendritic tree, will amplify some synapses in a biased manner. Additionally, like synapses may work in a coordinated manner with respect to their relative proximity. Coordination between noradrenergic and serotonergic synapses is less likely.

Co-Authorship

Dr. P. Ken Rose was my supervisor throughout this thesis, and as such, was instrumental in the design of the studies, as well as the data collection and analysis. Rebecca Cranham and Monica Neuber-Hess assisted in the surgical procedures described in the methods. Keith Fenrich, Dr. Clair Meehan, and Dr. P. Ken Rose assisted in the data collection involving intracellular motoneuron staining described in the methods. Monica Neuber-Hess also assisted in the histological procedures outlined in the methods. Colin Meyer-Macaulay fully reconstructed the motoneuron Sena 4-5. Emilie LaLonde wrote the program required to calculate distances between neighbouring contacts, described in Figure 3.8. I am responsible for the first draft of the thesis, and subsequent drafts included many comments and suggestions from Dr. P. Ken Rose and Keith Fenrich.

Acknowledgements

While I have spent the last 19 years of my life in school, these last two years have stood out above the rest. Not only has it been the most challenging and productive learning experience, it has also been the most enjoyable. I owe this experience to my supervisor Dr. P. Ken Rose. Thank you Dr. Rose, both for being a great teacher, and for the curiosity and energy that you channel towards every experiment and finding. While you have many qualities that one would desire in a supervisor, the main thing which has impacted my time in your lab has been your heartfelt care and concern for others around you. You are always there to talk to or to stay late at an experiment. Moreover, during these past couple months you have worked selflessly around the clock to send much-needed thesis revision to me, as late as 10:30 pm, or as early as 8:30 am (and sometimes both in the same day). I consider myself lucky to have worked with you, and look forward to another productive year in your lab.

The many individuals which have made up the Rose Lab during these past two years have been both an invaluable resource and great social company. In particular, thank you to Dr. Claire Meehan and Keith Fenrich. You were always willing to let me sit in on your experiments, and to answer hours of endless questions regarding those same experiments. You were also eager to help troubleshoot any difficulties that I was having, and offered copious amounts of constructive criticism regarding my work. Without your help, the rigor of my study, and my general understanding of many lab techniques, would not be what it is today. I can only hope that I can one day be as great of an aid to others, as you have been to me. Many others in the lab have also been a delight to be around,

and assisted me in many ways. Instead of making mention of all these individuals, I will only briefly say thank you to the Rose Lab as a whole, and everyone that has been part of it. The brevity of my thanks should not in any way be interpreted as anything less than the most sincere thanks and appreciation I have for the Rose Lab. To fully enumerate all of the contributions of these individuals would take longer than time or paper would allow.

I would also like to acknowledge the many other students and professors I have met during these past two years. Thank you to those students with whom I started my Masters in Neuroscience in the Fall of 2006. The company and conversations we shared over good food and drinks were an integral part of my Masters. You provided a forum to problem solve and trouble shoot, listening ears to stress about posters and presentations, and friends with whom to celebrate successful projects and events. I would also like to thank the professors whom I have had the privilege of knowing. Especially thank you Dr. Neil Magoski: You are an excellent teacher, who is responsible for most of what I have learned, and likely most of what I have forgotten, about receptors and channels. Not only did you aid me in the classroom setting, you always asked good questions during presentations, offered insightful papers to me, were available to talk to, and always asked about my progress with genuine interest. Thank you.

Lastly, I would like to thank Heather Elliott. I could not ask for a more amazing girlfriend. Thank you for listening to me ramble on and on about my project, even though you are in Art History. Thank you for proofreading my thesis, so that it was legible for Dr. Rose and Keith Fenrich to edit. Thank you for cooking me meals so that I

could make it through this thesis writing time without starving, and for putting up with me these last couple stressful months. You are always there to help me out, thank you.

Table of Contents

Abstract.....	ii
Co-Authorship.....	iv
Acknowledgements.....	v
Table of Contents.....	viii
List of Figures.....	x
List of Tables.....	xii
List of Abbreviations.....	xiv
List of Symbols.....	xv
Chapter 1 Introduction.....	1
1.1 Introductory Comments.....	1
1.2 Basic Features of the Input-Output Properties of Motoneurons.....	4
1.3 Dendritic Tree Structure.....	5
1.4 Transmission of Current by Dendrites.....	9
1.4.1 Cable Properties and the Conduction of Synaptic Current Along Dendrites ...	11
1.4.2 Interactions Between Synapses Acting on Ionotropic Receptors.....	12
1.4.3 Voltage-Dependent/Independent Channels on Dendrites.....	13
1.4.3.1 Part 1: Evidence for Voltage-Dependent/Independent Channels on Dendrites.....	13
1.4.3.2 Part 2: Interactions Between Synapses Acting on Ionotropic Receptors and Voltage-Dependent/Independent Channels.....	15
1.4.4 Modulation of Voltage-Dependent/Independent Channels by Neurotransmitters Acting on Metabotropic Receptors.....	18
1.5 Distribution of Synapses Acting on Ionotropic Receptors.....	23
1.6 Distribution of Synapses Acting on Metabotropic Receptors.....	24
1.7 Statement of Problem and the Goals.....	25
1.8 Statement of Goals.....	29
Chapter 2 Methods.....	30
2.1 Animal Preparation.....	30
2.2 Motoneuron Identification and Intracellular Injections.....	31

2.3 Perfusion and Tissue Processing.....	32
2.4 Reconstruction of Motoneuron Dendritic Trees.....	34
2.5 Identification of Contacts.....	35
Chapter 3 Results.....	36
3.1 Distribution of Contacts.....	36
3.2 Center of Mass (COM) Analysis.....	42
3.3 Proximal Versus Distal Gradients in the Distribution of 5-HT and NE Contacts...	47
3.4 Distribution of NE and 5-HT Contacts Relative to Other NE and 5-HT Contacts .	58
3.4.1 5-HT to 5-HT Contacts and NE to NE Contacts	58
3.4.2 NE to 5-HTContacts and 5-HT to NE Contacts	67
Chapter 4 Discussion	73
4.1 Methodological Considerations.....	74
4.1.1 Sample Size	74
4.1.2 Labeling of Contacts.....	76
4.1.3 Volume Transmission.....	77
4.1.4 Comparison of Observed Distributions to Diameter Weighted Distributions for Nearest Neighbour Analysis.....	78
4.2 Regions Devoid of NE and 5-HT Innervation	80
4.3 Preferential Innervation of Dorsal and Ventral Dendrites	81
4.4 Preferential Innervation of Small Diameter and Distal Dendrites	82
4.5 Importance of the Relative Proximity between NE and 5-HT contacts.....	84
4.5.1 Pairs of NE and of 5-HT Contacts are Located in Close Proximity.....	85
4.5.2 NE and 5-HT Contacts are Located Far from One Another.....	86
4.6 Conclusion.....	87
References.....	89

List of Figures

Figure 1.1 Motoneuron current-frequency relationship, in the absence of neuromodulatory input.....	2
Figure 1.2 Motoneuron current-frequency relationship, in the presence of monoaminergic input.....	3
Figure 1.3 Dendritic trees from different neuron types.....	7
Figure 1.4 Dendritic trees from different motoneuron types.....	8
Figure 1.5 Second messenger signal cascade associated with NE _{α1} and 5-HT _{2a/c} receptor activation.....	19
Figure 3.1 Confocal microscopy images of NE and 5-HT labeled boutons in contact with splenius motoneuron dendrites.....	38
Figure 3.2 Distribution of NE and 5-HT contacts on Sena 3-3.....	40
Figure 3.3 The density of NE and 5-HT contacts per 1000μm ² of dendritic surface area for each cell.....	43
Figure 3.4 Description of the COM analysis.....	46
Figure 3.5 Dendritic distance from soma versus the cumulative frequency of dendritic surface area, and number of NE and 5-HT contacts, for Sena 5-2.....	50
Figure 3.6 The proportion of contacts and dendritic surface area as a function of dendritic diameter.....	54
Figure 3.7 Comparison of the dendritic distances from soma to observed NE and 5-HT contacts on Sena 5-2 and NE and 5-HT contacts from a computer generated distributions that were diameter-weighted.....	56
Figure 3.8 Description of nearest neighbor analysis.....	62

Figure 3.9 Comparison of the volume between nearest neighbour pairs of observed NE and 5-HT contacts on Sena 5-2 and nearest neighbour pairs of NE and 5-HT contacts from computer generated distributions that were diameter-weighted (cf. Figure 3.6).....	64
Figure 3.10 Comparison of the volume between nearest neighbours of observed NE/5-HT contacts on Sena 5-2 and nearest neighbours of NE/5-HT contacts from computer generated distributions that were diameter-weighted (cf. Figure 3.6).....	68

List of Tables

Table 1.1 The major stages that link motoneuron input to output, and the factors that influence each stage.....	6
Table 1.2 Ionotropic and metabotropic receptors of motoneurons.....	10
Table 1.3 Voltage dependent/independent channels on motoneurons.....	14
Table 3.1 Morphological summary of all five reconstructed splenius motoneurons	37
Table 3.2 Summary of NE and 5-HT contacts for each motoneuron, reported as the absolute number and density with respect to dendritic surface area and dendritic length	41
Table 3.3A Summary of the X, Y, and Z coordinates of the observed COMs for 5-HT contacts, relative to the COM based on a uniform density of 7 synapses/100.....	48
Table 3.3B Summary of the X, Y, and Z coordinates of the observed COMs for NE contacts, relative to the COM based on a uniform density of 7 synapses/100 μm^2	49
Table 3.4A Proximal versus distal gradients in the distribution of NE contacts.....	52
Table 3.4B Proximal versus distal gradients in the distribution of 5-HT contacts.....	53
Table 3.5A Effect of the bias to small diameter dendrites by NE contacts on the proximal to distal gradient of the distribution of NE contacts.....	57
Table 3.5B Effect of the bias to small diameter dendrites by 5-HT contacts on the proximal to distal gradient of the distribution of 5-HT contacts.....	59
Table 3.6A Median volume between nearest neighbors of pairs of observed NE contacts and diameter-weighted, computer generated, contacts.....	65
Table 3.6B Median volume between nearest neighbors of pairs of observed 5-HT contacts and diameter-weighted computer generated, contacts.....	66

Table 3.7A Median volume between nearest neighbors of pairs of NE/5-HT contacts, and contacts selected from two, independent, computer generated, sets of contacts, distributed using a diameter-weighted algorithm. NE contacts were used as the reference.....69

Table 3.7B Median volume between nearest neighbors of pairs of NE/5-HT contacts, and contacts selected from two, independent, computer generated, sets of contacts, distributed using a diameter-weighted algorithm. 5-HT contacts were used as the reference.....70

List of Abbreviations

5-HT	Seorotonin	IPSP	Inhibitory postsynaptic potential
Ach	Acetylcholine	kg	Kilogram
AHP	After spike hyperpolarization	MF	Medial funiculus
BK	Big conductance Ca^{++} activated K^+ channels	mAHP	Medium AHP
		mm	Millimeter
cm	Centimeter	mg	Milligrams
CNS	Central nervous system	ml	Milliliter
D β H	Dopamine beta-hydroxylase	μ m	Micrometer
DAG	Diacyl glycerol	NE	Norepinephrine
DLF	Dorsal lateral funiculus	pH	Power of hydrogen
EPSP	Excitatory postsynaptic potential	PIC	Persistent inward current
fAHP	Fast AHP	SK	Small conductance Ca^{++} activated K^+ channels
GABA	gamma-aminobutyric acid	TASK	TWIK-related acid-sensitive K^+ channels
HCN	Hyperpolarization-activated cyclic nucleotide-gated	TWIK	Tandem P domains in a weak inwardly rectifying K^+ current
IP3	Inositol trisphosphate		

List of Symbols

A	Amp
Ca^{++}	Calcium ion
E_{rev}	Reversal potential
g	Conductance
i	Current
i_{syn}	Synaptic current
i_{soma}	Somatic current
K^{+}	Potassium ion
KCl	Potassium Chloride
$\text{M}\Omega$	Mega Ohms
Na^{+}	Sodium ion
Ω	Ohms
π	Pi
V	Voltage
V_m	Membrane potential

Chapter 1

Introduction

1.1 Introductory Comments

Over 100 years ago, Sherrington (1906) described the motoneuron as the ‘final common pathway’. This description highlights the unique role of the motoneuron: it is the only route by which descending and segmental motor signals can be transmitted to skeletal muscles, the effectors of movement. Thus, a comprehensive explanation of when and how the motoneuron is activated is critical to our understanding of how descending motor commands and feedback from peripheral receptors are converted into purposeful movement. When and how the motoneuron is activated is determined by multiple factors: As shown in Figure 1.1, the current generated by activation of ionotropic receptors increases or decreases motoneuron activity in a piecewise linear manner (Granit et al. 1963; 1966; Schwindt & Calvin, 1973). However, this relationship is not fixed. Instead, it can be dynamically altered via the actions of metabotropic receptors that act on voltage-dependent and -independent channels. These actions can either change the threshold current for evoking rhythmic discharge or change the slope of the current-frequency relationship, as shown in Figure 1.2 (Hounsgaard & Kiehn, 1989; Lee & Heckman, 1998a, 1998b, 1999, 2000; Hornby et al. 2002; Dai et al. 2002; Lee et al. 2003; Gilmore & Fedirchuk, 2004; Heckman et al. 2004; Harvey et al. 2006a; 2006b; 2006c; Manuel et al. 2006; Miles et al. 2007).

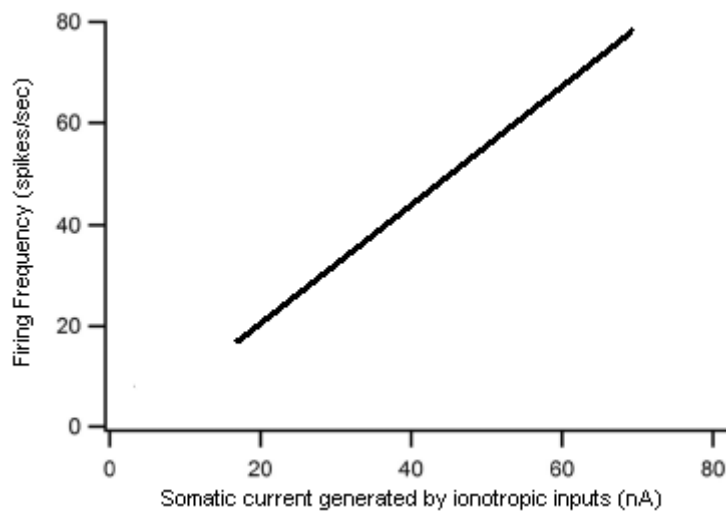


Figure 1.1 Motoneuron current-frequency relationship, in the absence of neuromodulatory input. This figure is adopted from data provided by Granit et al. (1963 & 1966) and Schwindt & Calvin (1973).

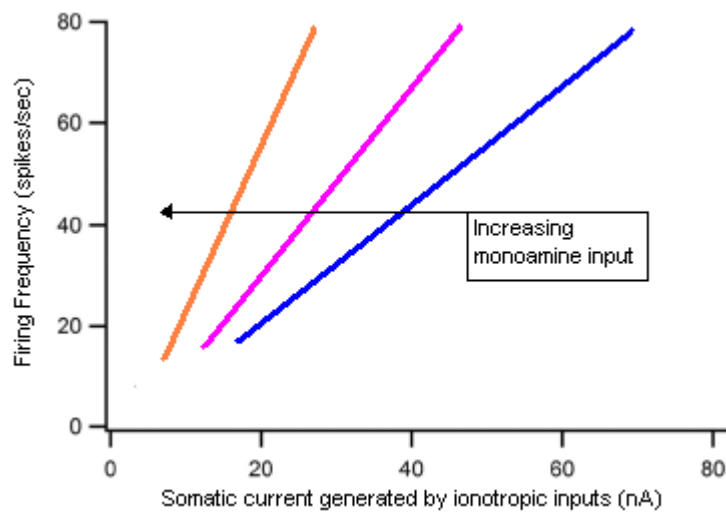


Figure 1.2 Motoneuron current-frequency relationship in the presence of monoaminergic input. This figure is adopted from a review by Heckman et al. (2003).

This thesis describes the distribution of synapses from two descending systems on the dendritic trees of feline splenius motoneurons. Both systems release neurotransmitters that act on metabotropic receptors. Synapses from one of the descending systems release serotonin (5-HT), and synapses from the other descending system release norepinephrine (NE). This study is founded on the hypothesis that the control of motoneuron input-output properties (i.e. when and how motoneurons are activated) depends on the location of these synapses on the dendritic tree.

1.2 Basic Features of the Input-Output Properties of Motoneurons

The input to motoneurons is commonly defined as the activity of all axons that form synapses on the motoneuron and release neurotransmitters that act on ionotropic receptors. The binding of neurotransmitters to ionotropic receptors opens ligand-dependent channels that allow positive or negative current to flow out of or into the motoneuron. The amount of current is determined by the number, type, and discharge frequency of active synapses, as well as the number and properties of the ligand-gated channels. Most synapses on motoneurons are located on the dendritic tree. Thus, the current generated at each synapse must travel along one or more dendritic branches before reaching the soma and initial segment. Along this route, some current will be lost due to the inherent leakiness of neuronal membranes. The magnitude of this loss will be determined by the morphology of the dendritic tree and the state of voltage-dependent or voltage-independent channels in the dendritic membrane. These channels are often influenced by neurotransmitters that act on metabotropic receptors. In some cases, there

may be a net gain in current depending on which channels are activated or inactivated.

Motoneuron output is defined as the temporal pattern of action potentials that are generated at the initial segment and travel down the axon to muscle fibers. This pattern is determined by the magnitude and time course of the current reaching the initial segment and the distribution, type, and state of the voltage-dependent and independent channels found on the soma and initial segment. Table 1.1 summarizes the major steps that link motoneuron input to output and the factors that influence each step.

1.3 Dendritic Tree Structure

Motoneurons have the largest dendritic trees of all neurons in the central nervous system (CNS) (Segev, 1998). As shown in Figure 1.3, a typical dendritic tree of a motoneuron dwarfs the dendritic trees of other types of neurons. Detailed reconstructions of motoneurons demonstrate that the soma gives rise to 7-15 primary dendrites, each having several orders of branching prior to termination more than 1000 μm from the soma (Rose, 1981; Ulfhake & Kellerth, 1981; Burke et al. 1982; Keirstead & Rose, 1983; Cameron et al. 1985; Rose et al. 1985; Bras et al. 1987; Cullheim et al. 1987; Kernell & Zwaagstra, 1987; Fukunishi et al. 1999; Bui et al. 2003; Moritani et al. 2003; Rose & Cushing, 2004). The shape of the dendritic tree depends on both which muscle the motoneuron innervates, and the motoneuron's location within the spinal cord. For example, the dendritic trees of triceps surae motoneurons in the lumbar spinal cord are usually spherical, while the dendritic trees of trapezius motoneurons in the upper cervical cord are cylindrical Figure 1.4.

Table 1.1 The major stages that link motoneuron input to output, and the factors that influence each stage.

Stage:	Input	Conduction	Generation of Output
Influencing Factors:	<ul style="list-style-type: none"> - Distribution of active synapses - Frequency of active synapses - Type of synapses active - Density and type of ionotropic receptors 	<ul style="list-style-type: none"> - Dendritic tree morphology - Synaptic location on dendritic tree - Distribution and type of channels along the dendrite - Current state of channels, determined largely by neuromodulation 	<ul style="list-style-type: none"> - Distribution and type of membrane bound channels along the soma/initial segment - Current state of channels, determined largely by neuromodulation

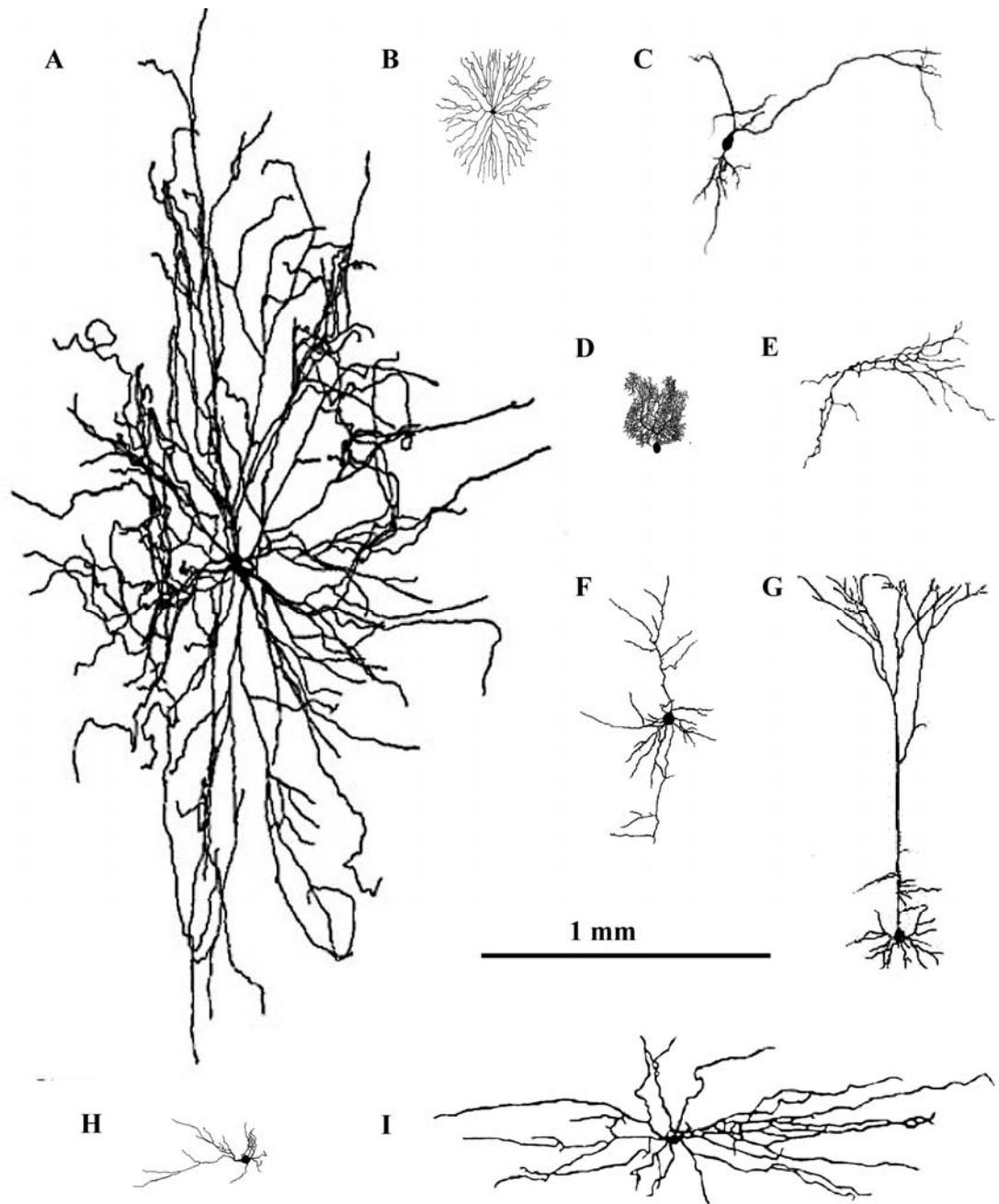


Figure 1.3 Dendritic trees from different neuron types. All cells are shown at the same scale. A) Feline splenius motoneuron (Bui et al. 2003) B) Rabbit starburst retinal amacrine cell (Bloomfield & Miller, 1986) C) Rat substantial nigra dopamine cell D) Rat cerebellar purkinje cell (Vetter et al. 2001) E) Feline renshaw cell (Bui et al. 2003) F) Mouse layer 3 pyramidal cell (García-López et al. 2006) G) Rat layer 5 pyramidal cell (Vetter et al. 2001) H) Rat genioglossal motoneuron (Núñez-Abades et al. 1994) I) Feline Ia inhibitory interneuron (Bui et al. 2003).

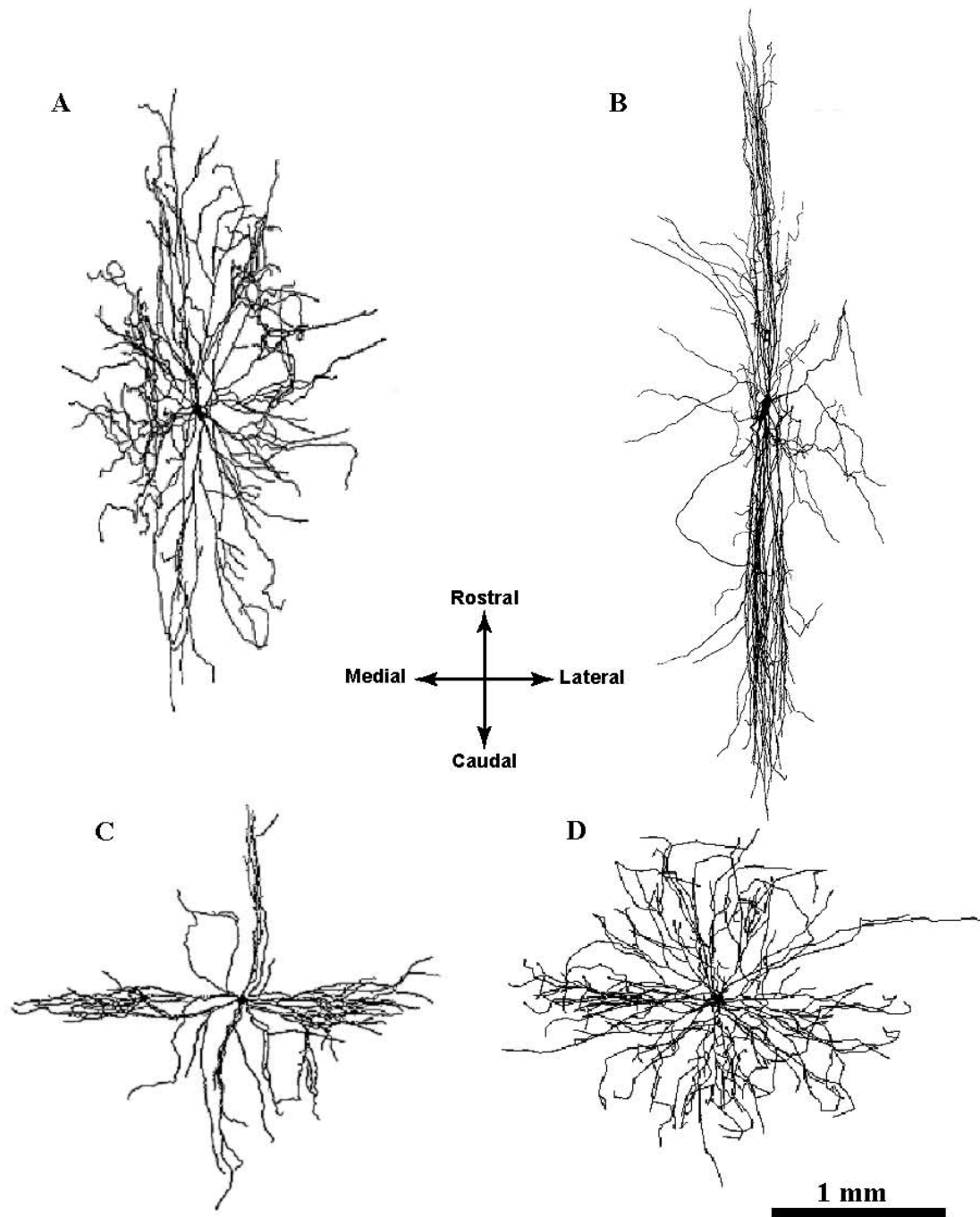


Figure 1.4 Dendritic trees from different motoneuron types. All cells are shown at the same scale. A) Feline splenius motoneuron (Bui et al. 2003) B) Feline trapezius motoneuron (Vanner & Rose, 1984) C) Feline phrenic motoneuron (Cameron et al. 1991) D) Feline hindlimb motoneuron (Brown & Fyffe, 1981).

It has been estimated that the dendritic tree of a single motoneuron receives 20,000 to 50,000 synapses (Conradi et al. 1979; Ulfhake & Cullheim, 1988; Rose & Neuber-Hess, 1991; Brännström, 1993). These synapses release neurotransmitters, which act on ionotropic and metabotropic receptors, summarized in Table 1.2 (based on Rekling et al. 2000). Ionotropic receptors also serve as channels and are often called ligand-gated channels. When a ligand binds to the receptor, the channel opens and allows current to flow across the cell membrane in the form of ions. The current that one synapse generates is equal to the total conductance of that synapse (the sum of the conductance of each channel in the post-synaptic membrane), multiplied by the driving potential. This relationship is demonstrated by the following equation:

$$i_{\text{syn}} = g(E_{\text{rev}} - V_m)$$

where i_{syn} is the current generated, g is the total conductance, E_{rev} is the reversal potential of the ion or ions moving across the channel, and V_m is the post-synaptic membrane potential. In contrast, when a ligand binds to a metabotropic receptor, it activates G-proteins which modulate a wide variety of voltage-dependent and independent channels (Lodish et al. 2000).

1.4 Transmission of Current by Dendrites

Over 95% of the synapses on motoneurons are located on the dendritic tree (Burke et al. 1982; Ulfhake & Kellerth, 1984; Cameron et al. 1985; Rose et al. 1985; Bras et al. 1987; Cullheim et al. 1987; Kernell & Zwaagstra, 1989; Rose et al. 1991; Fukunishi et al. 1999; Moritani et al. 2003). Thus, the current generated by these synapses,

Table 1.2 Ionotropic and metabotropic receptors on motoneurons. This table is based on data review by Rekling et al. (2000).

Ionotropic Receptors	Receptor Agonist	Metabotropic Receptors	Receptor Agonist
AMPA	Glutamate	Group 1-3 mGlu receptors	Glutamate
Kainate	Glutamate	GABA _b receptors	GABA
NMDA	Glutamate	D1 and D2 receptors	Dopamine
GABA _{a&c} receptors	GABA	Muscarinic 2 Ach receptor	Acetylcholine
Glycine receptors	Glycine	Alpha1 receptors	Norepinephrine
		5-HT _{2a&c} receptors	Serotonin
		P _{2x}	ATP
		Adenosine 1-3 receptors	Adenosine
		TRHR1&2	TRH
		NK ₁₋₃	Neurokinines (including Substance P)
		V _{1a}	Arginine Vasopressin

regardless of its source (e.g. ligand-dependent channels or voltage-dependent/independent channels activated by metabotropic receptors) must travel for some distance along the dendrite before reaching the soma and the spike initiation zone at the initial segment. The amount of current that reaches the soma is determined by: (1) the cable properties of dendrites, (2) interactions between synapses acting on ionotropic receptors and (3) activation or inactivation of voltage-dependent/independent channels.

1.4.1 Cable Properties and the Conduction of Synaptic Current Along Dendrites

Cable theory is widely used to describe the biophysical principles that govern the flow of current en route from synaptic sites on the dendritic tree to the soma (Rall, 1967). Assuming that the dendritic membrane is passive (i.e., the electrical properties of the membrane are fixed), this theorem approximates a dendrite as a core conductor consisting of a thin insulating tube of membrane filled with an inner conducting medium (Rall, 1977). However, the membrane is not a perfect electrical insulator, and, coupled with the inherent resistance of the cytoplasm, this leads to the loss of synaptic current through the membrane en route to the soma (Koch, 1984). Synaptic current is also lost as it spreads distally from the synapse. Branch points en route to the soma also introduce additional paths for current loss. Simulations based on compartmental models, incorporating detailed measurements of motoneuron dendritic tree geometry, have suggested that the current lost en route to the soma can be as high as 80%, but typically is closer to 25 to 40% (Rose & Cushing 1999, Korogod et al. 2000; Powers & Binder 2001, Bui et al.

2003; Cushing et al. 2005). The magnitude of current loss is strongly related to the distance between the synapse and the soma.

1.4.2 Interactions Between Synapses Acting on Ionotropic Receptors

The current generated by the opening of ligand-gated ion channels in the membrane is highly dependent on the driving potential, as noted above, and restated below.

$$i_{\text{syn}} = g(E_{\text{rev}} - V_m)$$

E_{rev} for a given ion will not change significantly when multiple synapses are active. However, activation of a single synapse will change the local V_m . This will alter the driving potential at nearby synapses. Thus, the total current generated by simultaneous activation of multiple nearby synapses will be less than the predicted linear sum (Koch et al. 1983; Segev & Parnas, 1983). Simulations based on anatomically realistic models suggest that the current lost due to sublinear summation synaptic currents on motoneurons is as large, or larger, than the current lost due to cable properties (Cushing et al. 2005).

Locally coactive synapses on distal small diameter dendrites will behave differently than those on proximal large diameter dendrites. For a given input of current, a small diameter dendrite will experience a larger voltage change than a large diameter dendrite. This voltage change can be more than 10 fold greater on small diameter dendrites as opposed to those of a large diameter (Rall, 1967; Barrett & Crill, 1974). The change in membrane voltage will effect the driving potential for ionotropic channels at

nearly synapses. The magnitude of interactions between nearby synapses will therefore be greater on small diameter dendrites than large diameter dendrites.

1.4.3 Voltage-Dependent/Independent Channels on Dendrites

1.4.3.1 Part 1: Evidence for Voltage-Dependent/Independent Channels on Dendrites

The application of cable theory noted above assumes that the dendritic membrane is passive. This is unlikely. There is mounting evidence that the dendrites of motoneurons, like those of other cells, possess several types of voltage-dependent and independent channels that dynamically change the electrical properties of the membrane. These channels add another layer of factors that determine the transmission of current to the soma.

As summarized in Table 1.3, there are at least 11 different types of voltage-dependent channels and 4 types of voltage-independent channels (e.g. TASK-1 channels) on motoneurons. Most of the known channel locations are somatic. However, there is very persuasive anatomical and/or electrophysiological evidence that L-type Ca^{++} , persistent Na^+ , $\text{Kv} 2.1$, and SK (small conductance Ca^{++} activated K^+ channels) channels are located on the dendritic trees of motoneurons. Descriptions of the dendritic distribution of the other 11 channels are currently either cursory or absent. Moreover, most of the known distributions are described in terms of dendritic versus somatic. The absence of a detailed account of the dendritic distribution of voltage-dependent and independent channels has hindered efforts to determine their role in the control of motoneuron input-output properties.

Table 1.3 Voltage dependent/independent channels on motoneurons. This table is based on data from a variety of sources. (Alessandri-Haber et al. 2002; Ballou et al. 2006; Berg et al. 2004; Carlin et al. 2000; Li and Bennett, 2003; 2007; Jones & Lee, 2006; Burke et al. 2003; Milligan et al 2006; Moritz et al. 2007; Rekling et al. 2000; Simon et al. 2003; Westenbroek et al. 1998).

Voltage-dependent channels	Voltage-independent channels
I_{Na}	TASK-1/3
$I_{Na-Persistent}$	$I_{Ca BK}$
$I_K Kv 1.6$	$I_{Ca SK}$
$I_K Kv 2.1$	$I_{K Na}$
$I_K Kv 3.1/3$	
$I_K Kv 4.2/3$	
I_{Ca-L}	
$I_{Ca-P/Q}$	
I_{Ca-N}	
I_h	
$I_{K IR}$	

In theory, this feature is best described using anatomical techniques based on immunocytochemistry (e.g. see Lorincz et al. 2002). However, few studies have used these techniques to quantitatively examine the distribution of channels over the entire dendritic tree.

As a complement to immunocytochemistry, several groups have developed strategies to map the distribution of voltage-dependent channels based on computational models of motoneurons (Elbasiouny et al. 2005, 2006; Bui et al., 2006; Grande et al. 2007a; Shapiro & Lee, 2007). Predictions based on these models suggest that L-type Ca^{++} channels are restricted to ‘hotspots’, approximately 100 μm long (Bui et al. 2006). The distance between the hotspots and the soma varied from 180 to 850 μm and increased with the size of the motoneuron (Elbasiouny et al. 2005; Grande et al. 2007a).

1.4.3.2 Part 2: Interactions Between Synapses Acting on Ionotropic Receptors and Voltage-Dependent/Independent Channels

Voltage-dependent/independent channels can serve to either amplify or dampen the delivery of synaptic current generated en route to the soma. Amplification may provide a means to counteract the problem of current attenuation caused by cable properties and sublinear summation (Migliore & Shepherd, 2002).

Persistent inward currents (PICs) were first described for motoneurons over 30 years ago by Schwindt & Crill (1977). In the past decade PICs have emerged as one of the primary means by which motoneurons amplify synaptic currents (Heckman et al. 2003). PICs consist of dihydropyridine-sensitive L-type Ca^+ channels (CaV1.3 and possibly CaV1.4 see, Barrett & Crill, 1980; Hounsgaard & Kiehn, 1989; Koschak et al.

2003; Li & Bennett, 2003) and a persistent Na^+ current. However, the class of Na^+ channels responsible for this current is unknown (Lee & Heckman, 2001; Li & Bennett, 2003, Li et al. 2004).

L-type Ca^{++} channels can be activated by excitatory synaptic activity or deactivated by inhibitory synaptic activity (Hounsgaard et al. 1988; Hounsgaard & Kiehn, 1989; Lee & Heckman, 1996; Lee & Heckman, 1998; Prather et al. 2001; Hultborn et al. 2003; Lee et al. 2003; Elbasiouny et al. 2005; Elbasiouny et al. 2006; Bui et al. 2006; Hyngstrom et al. 2007; Grande et al. 2007a, 2007b). The opening of L-type Ca^{++} channels causes an influx of Ca^{++} . Ca^{++} PICs will therefore amplify synaptic current en route to the soma, to either initiate or increase the firing frequency, (Heckman et al. 2008; Housgaard et al. 1984). The influx of Ca^{++} causes a steady depolarization (Schwindt & Crill, 1980), later referred to as a plateau potential (Hounsgaard et al. 1984; Hounsgaard & Kiehn, 1989). Since L-type Ca^{++} channels are slow to inactivate, the plateau potential will remain long after the removal of synaptic input. Thus, the motoneuron will continue to discharge in the absence of a sustained excitatory synaptic activity until the arrival of inhibitory synaptic activity. If this input hyperpolarizes the region of the motoneuron with the L-type Ca^{++} channels, the channels will deactivate and the motoneuron will stop firing (as reviewed by, Heckman et al. 2008).

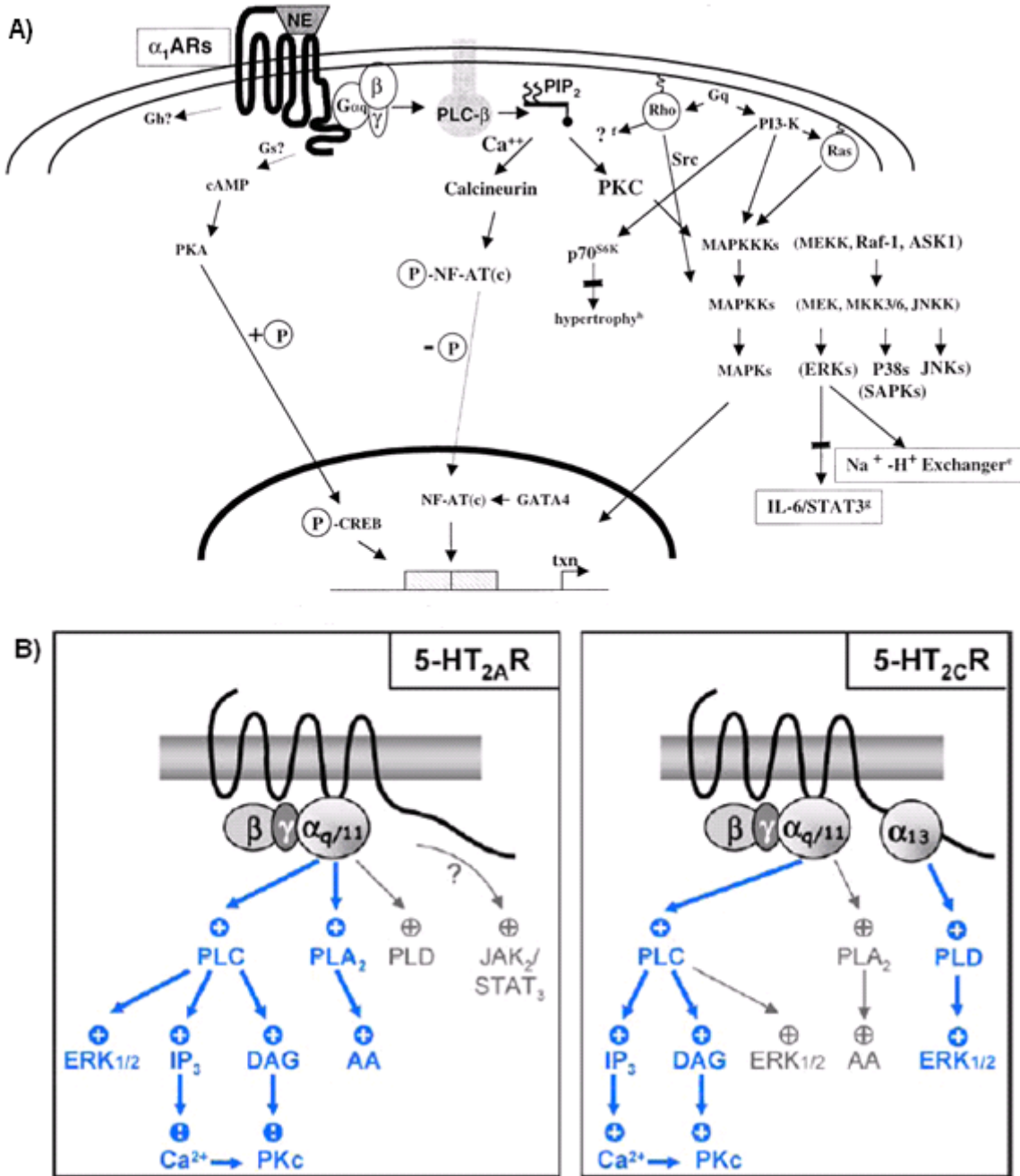
There are many other voltage dependent/independent channels that regulate the delivery of synaptic current to the somata of motoneurons. Persistent Na^+ channels act in a similar way as L-type Ca^{++} channels. However, these channels have a much smaller time constant than L-type Ca^{++} channels, allowing persistent Na^+ channels to open much

more rapidly. Therefore, transient synaptic activity that is too brief to open L-type Ca^{++} channels can activate persistent Na^+ channels. TASK channels (TWIK-related acid-sensitive K^+ channels, where TWIK is an acronym for tandem P domains in a weak inwardly rectifying K^+ current) cause a tonic outward K^+ current. Activation of these channels increases the membrane's permeability to K^+ and thus increasing membrane 'leakiness' (Talley & Bayliss, 2000; Bayliss et al. 2003). Increasing the 'leakiness' of the membrane will increase the magnitude of current attenuation. Ca^{++} activated small conductance K^+ channels (SK) cause an outward current. Some SK channels are in close proximity to L-type Ca^{++} channels (Li & Bennett, 2003). In these circumstances, activation of the SK channels will counteract the inward current generated from Ca^{++} PICs and limit the magnitude of the depolarization caused by Ca^{++} PICs. HCN1 (Hyperpolarization-activated cyclic nucleotide-gated) channels cause an inward mixed-cation current, referred to as the I_h current. HCN1 channels are deactivated with tonic excitatory (depolarizing) input, and are activated with tonic inhibitory (hyperpolarizing) input. HCN1 channels therefore counteract synaptic currents, reducing both the depolarization caused by tonic activation of excitatory synapses or the hyperpolarization caused by tonic activation of inhibitory synapses. Transient synaptic inputs, however, will be unaffected because HCN1 channels take at least 30 msec to be activated or deactivated (as reviewed by, DiFrancesco & Borer, 2007; Hsiao et al. 1997).

1.4.4 Modulation of Voltage-Dependent/Independent Channels by Neurotransmitters Acting on Metabotropic Receptors

The properties of many voltage dependent/independent channels are modulated by the actions of metabotropic receptors. Activation of these receptors leads to the dissociation of G protein subunits, which diffuse through the cytoplasm, activating various other proteins (Figure 1.5). These proteins form a second messenger signal cascade that alters the function of many proteins, including voltage-dependent and independent channels, primarily through phosphorylation or dephosphorylation. Phosphorylation or dephosphorylation of voltage-dependent and independent channels serves to change the response of the channels to excitatory or inhibitory synaptic activity. Some channels on motoneurons, such as L-type Ca^{++} channels, are largely unresponsive to excitatory or inhibitory inputs in the absence of serotonin, glutamate, acetylcholine, or noradrenalin, acting via metabotropic receptors (Hounsgaard et al. 1988; Hounsgaard & Kiehn, 1989; Delgado-Lezama et al. 1997; Hsiao et al. 1998; Svirskis and Hounsgaard, 1998; Lee and Heckman, 1999; 2000; Perrier and Hounsgaard, 2003; Alaburda & Hounsgaard, 2003; Harvey et al. 2006b; 2006c; Rank et al. 2007). Thus, the factors that influence the transmission of current along a dendrite involve the actions of metabotropic receptors in addition to the activity of inhibitory/excitatory synapses and voltage-dependent and independent channels. Unlike the effects of ionotropic receptors, the time course of the actions of metabotropic receptors can range from milliseconds (i.e. phosphorylation of a channel to shift its voltage dependency) to days (involving altering gene transcription at the soma). These effects depend on the characteristics of the

Figure 1.5 Second messenger signal cascade associated with NE_{alpha1} and 5-HT_{2a/c} receptor activation. A) Signal cascade resulting from NE_{alpha1} receptor activation. This figure was adopted from Michelotti et al. 2000. B) Signal cascade resulting from 5-HT_{2a/c} receptor activation. This figure was adopted from Bockeaert et al. 2006.



second messenger proteins at the site of the metabotropic receptor, as well as the properties of voltage-dependent and independent channels (effectors) within the range of the second messengers.

It is well established that metabotropic receptors activated by NE and 5-HT play an important role in the regulation of motoneuron input-output properties. 5-HT receptors are subdivided into seven different families (5-HT₁₋₇). Many of these families have multiple subtypes of receptors, such as 5-HT_{1a-c} (Fink & Göthert 2007). These receptors can be either ligand-gated or metabotropic, and can also be either excitatory or inhibitory. Only 5-HT_{2a} and 5-HT_{2c} receptors are found on mammalian motoneurons (Hsiao et al. 1997, Harvey et al. 2006; Fink & Göthert 2007). Thus, the application of specific 5-HT_{2a} and 5-HT_{2c} receptor antagonists will block all of the effects of 5-HT on motoneurons (Hsiao et al. 1997; Fink & Göthert 2007). The 5-HT₂ receptor family (originally called 5-HT_{1c}) consists entirely of metabotropic receptors (Fink & Göthert 2007). 5-HT_{2a/c} receptors are both coupled to the same specific type of G protein, G_{q/11} (Fink & Göthert 2007). Activation of this protein initiates a signaling pathway that acts through the activation of inositol trisphosphate (IP₃) and diacylglycerol (DAG), as seen in Figure 1.5, and is known to increase the excitability of motoneurons.

5-HT increases the excitability of motoneurons. This action is partially mediated by modulation of L-type Ca⁺⁺ channels and this leads to an amplification of synaptic currents en route to the soma (Hounsgaard & Kiehn; 1985 & 1989; Perrier et al. 2002; Harvey et al. 2006a). Ca⁺⁺ PICs are not present in the absence of 5-HT, and other neuromodulators (Heckman et al. 2003, Harvey et al. 2006b). Persistent Na⁺ channels

are also modulated by 5-HT and this modulation increases Na^+ PICs that in turn amplify synaptic currents (Harvey et al., 2006a; 2006b).

5-HT also has a variety of effects on other channels, many of which are located at the soma. Modulation of persistent Na^+ channels on the soma by 5-HT controls the response of the motoneuron to sustained excitatory synaptic activity. 5-HT facilitates the activation of persistent Na^+ channels and this enables the motoneuron to discharge rhythmically for the duration of the synaptic activity (Harvey et al. 2006a). TASK-1 channels are inactivated by 5-HT_{2a/c} receptors coupled to $G_{q/11}$ proteins (Talley & Bayliss, 2000; Sirois et al. 2002; Perrier et al. 2003). Inactivation of TASK-1 channels will reduce the leakiness of the membrane, and therefore reduce the attenuation of synaptic current en route to the soma. 5-HT has also been shown to decrease the AHP, presumably by inhibiting Ca^{++} dependent K^+ channels (Wallén et al. 1989a; 1989b; Grunnet et al. 2004). This should increase firing frequency. This action of 5-HT has been demonstrated in turtle and lamprey motoneurons, but not in any mammalian motoneurons. The threshold of initiation for action potentials in the initial segment is also modulated by 5-HT. 5-HT hyperpolarizes the voltage threshold for action potentials and therefore increases neuronal excitability (Gilmore & Fedirchuk, 2004; Fedirchuk & Dai, 2004).

NE has 2 main families of receptors: alpha and beta. The beta receptors have 3 subtypes, beta₁₋₃, which are found in heart, lung, and adipose tissue respectively (Hayar et al. 2001). The alpha receptors have two subtypes, alpha_{1&2}. Alpha₂ receptors have 3 subtypes, alpha_{2a/b/c}. All of these receptors activate inhibitory G-Protein coupled receptors (Gi), and are found primarily on pre-synaptic membranes. The alpha₁ receptor family

also has three subtypes, $\alpha_{1a/b/d}$, and are all excitatory (Gq) (Hayar et al. 2001). The effects of NE on motoneurons are completely blocked by α_1 antagonists, and mimicked by α_1 agonists (Harvey et al. 2006). This suggests that α_1 receptors are the only family of NE receptors on motoneurons. The α_1 receptor is coupled to the same G-protein as the 5-HT_{2a/c} receptors, the Gq/11 protein. Therefore, NE will mediate its effects through a similar second messenger system as 5-HT, seen in Figure 1.5.

NE α_1 receptors regulate several types of channels on motoneurons. α_1 receptor activation, have been shown to modulate L-Type Ca^{++} channels and persistent Na^+ channels similar to 5-HT_{2a/c} receptor activation, allowing Ca^{++} and Na^+ PICs to be more readily activated by excitatory synaptic current (Perrier et al. 2002; Harvey et al. 2006b). Activation of α_1 receptors also inhibits TASK channels, similar to 5-HT_{2a/c} receptor activation (Parkis et al. 1995). NE has been shown to decrease the AHP time course, (Hayar et al. 2001; Fung & Barnes, 1987; Martinez-Pena y Valenzuela et al. 2004) again similar to 5-HT, (Franceschetti et al. 2003). This will increase maximum firing frequency. The threshold of initiation for action potentials in the initial segment is also modulated by NE. Similar to 5-HT, NE hyperpolarizes the voltage threshold for an action potential and this increases neuronal excitability (Gilmore & Fedirchuk, 2004; Fedirchuk & Dai, 2004).

It must be noted that many neurotransmitters, including NE and 5-HT, regulate transcriptional events, and in turn alter protein expression (Maronde et al. 1997; Matsumoto & Yoshioka, 2001; Duman, 1998). This regulation is often mediated by the cytoplasmic phosphorylation of CREB, which is achieved by cAMP activation of PKA

(Maronde et al. 1997; Matsumoto & Yoshioka 2001; Duman, 1998). However, the direct impact of long-term changes in protein expression on input-output properties of motoneurons is unknown.

1.5 Distribution of Synapses Acting on Ionotropic Receptors

There is a growing body of evidence that synapses affecting ionotropic receptors are arranged in highly organized patterns on the dendritic tree. For instance, synapses from Ia afferents are widely distributed throughout the dendritic tree on hind limb motoneurons that supply ankle extensor muscles (Brown & Fyffe, 1981; Fyffe & Light, 1984; Burke and Glenn, 1996). A comprehensive quantitative analysis by Burke and Glenn (1996) has shown that the density of these contacts on most dendrites is proportional to the available surface area (the exception being the dendrites projecting in the ventromedial- dorsolateral axis). In contrast, contacts from Ia afferents on cranial motoneurons have a strong proximal bias (Yabuta et al. 1996). This preference for proximal dendrites is also a feature of contacts from Renshaw cells (Fyffe, 1991). Renshaw cells provide recurrent inhibition to motoneurons, and innervate proximal regions of the dendritic tree (Fyffe, 1991). Over 93% of the synapses are within 65-470um from the soma. The most extreme example of a proximal bias is provided by synapses from Ia inhibitory interneurons. These synapses are found almost exclusively on the somata of motoneurons (Burke et al. 1971, Fyffe 1991, Alvarez & Fyffe, 2001). Other distribution patterns are equally restrictive, and are not always based on proximal versus distal dendrites. Some patterns are based on the orientation of the dendrites. For

example, vestibulospinal axons originating from the lateral vestibular nucleus preferentially terminate on rostrally or caudally directed dendrites of motoneurons that supply dorsal neck muscles (Rose et al. 1995). Other patterns are based on the relative position of the dendrites with respect to the soma in the ventral horn. Grande et al. (2005) has found that excitatory vestibulospinal axons that arise from neurons in the descending vestibular nucleus preferentially terminate on dendrites that lie medial to the somata of motoneurons that supply dorsal neck muscles. Thus, although the pattern of the synapse distribution may vary between afferent systems, all patterns are highly ordered.

1.6 Distribution of Synapses Acting on Metabotropic Receptors

The distribution of 5-HT synapses on the dendrites of motoneurons appears to depend on the type of motoneuron. The 5-HT innervation of motoneurons in the trigeminal motor nucleus that innervate jaw muscles is biased to proximal dendrites (Nagase et al. 1997). In contrast, 5-HT innervation of hind limb motoneurons is distributed throughout the dendritic tree and soma, with no regions of preferential innervation, e.g. proximal dendrites (Alvarez et al. 1998). 5-HT innervation of laryngeal motoneurons is primarily directed to proximal dendrites of cricoarytenoid motoneurons, but most 5-HT synapses on cricothyroid motoneurons are found on distal dendrites (Sun et al. 2002). The primary source of serotonin to motoneurons is from descending axons originating from neurons in the raphe nuclei, which are implicated in posture control (Kiehn et al. 1992; Yates et al. 1993; Jacobs & Fornal, 1997).

The distribution of NE synapses on the dendritic trees of alpha motoneurons is not known. It is known that neurons in the locus coeruleus and subcoeruleus are the sole source of NE projections to the spinal cord and that many NE synapses are found near large neurons, presumably alpha motoneurons, in lamina IX of the ventral horn (Westlund et al. 1984). The distribution on gamma motoneurons has been described (Gladden et al. 2000). The NE innervation of gamma motoneurons is widely distributed on the dendritic tree, and includes the soma. NE contacts were consistently less abundant than 5-HT contacts on the same cell (only 53-62% of the 5-HT frequency). The precise role of the locus coeruleus-NE projections to motoneurons, beyond amplification of synaptic currents, remains unclear. However, it is well known that the locus coeruleus-NE system as a whole plays a key role in arousal, and recent studies suggest that it may also regulate adaptive behaviour by controlling the balance between exploiting known sources of reward and exploring the environment (Aston-Jones & Cohen, 2005).

1.7 Statement of Problem and the Goals

The input-output properties of motoneurons are not static. Instead, the discharge of motoneurons in response to the same input varies, depending on the state of several neuromodulator systems (Hounsgaard et al. 1986; Hounsgaard & Kiehn, 1989; Lee & Heckman, 1998a; 1998b; 1999; 2000; 2005; Hornby et al. 2002; Dai et al. 2002; Lee et al. 2003; Gilmore & Fedirchuk, 2004; Heckman et al. 2003; 2004; Harvey et al. 2006a, 2006b; 2006c; Manuel et al. 2006; Miles et al. 2007). For example, the strength of motor commands conveyed by descending spinal pathways or feedback signals from peripheral

receptors can be amplified several fold by 5-HT and NE (Hultborn & Kiehn, 1989; Heckman et al. 2003; 2005; Lee & Heckman, 2000). These neurotransmitters bind to NE_{α1} and 5-HT_{2a/c} receptors. These metabotropic receptors activate similar second messenger systems that, in turn, modulate a variety of voltage-dependent and independent channels. These channels are responsible for several types of currents, including, Na⁺ and Ca⁺⁺ PICs, Ca⁺⁺ activated K⁺ currents responsible for the AHP, leak K⁺ currents, and hyperpolarization activated currents (Perrier et al. 2002; Harvey et al. 2006a; 2006b; Berger, 1995; Hayar et al 2001; Fung & Barnes 1987; Martinez-Pena y Valenzuela et al. 2004; Talley & Bayliss, 2000; Sirois et al. 2002; Perrier et al. 2003). The net result is a highly dynamic relationship between the activity of afferents that relay motor or feedback signals to motoneurons and the discharge frequency of motoneurons. A comprehensive description of the mechanisms that control this relationship is fundamental to understanding the execution of purposeful movements and may provide important clues for understanding motor dysfunction following stroke and spinal cord injury (Heckman et al. 2005).

This study examines a subset of the mechanisms that regulate motoneuron input-output properties. All of these mechanisms share a common feature: the distribution of 5-HT and NE synapses on the dendritic tree of motoneurons. The distributions of 5-HT and NE synapses are described from two perspectives, global and local.

The global perspective is based on the hypothesis that the distributions of 5-HT and NE synapses are designed to amplify selected motor/feedback signals. This hypothesis predicts that 5-HT and/or NE synapses will be arranged in a non-uniform

manner, so that some dendrites, such as those that project rostrally or caudally, receive more synapses than dendrites that project in other directions. We have tested this prediction by quantitatively examining the distribution of axon terminals containing 5-HT or NE which contact the dendrites of motoneurons innervating the splenius muscle, a dorsal neck muscle. Splenius motoneurons were chosen deliberately because the dendrites of these cells are known to receive connections from vestibulospinal axons that preferentially innervate select regions of the dendritic tree (Rose et al. 1995; Grande et al. 2005; Grande et al. 2007). Thus, a key pre-requisite for selective amplification based on the global distribution of 5-HT or NE synapses, namely a non-uniform innervation by synapses conveying specific motor-related signals, is satisfied. Whether the distribution of 5-HT and NE synapses on splenius motoneurons is also non-uniform, is unknown. It is known that the distribution of 5-HT synapses depends on the type of motoneuron. 5-HT synapses are widely distributed throughout the dendritic tree of motoneurons that supply ankle extensors (Alvarez et al. 1998). In contrast, the distribution of 5-HT synapses on motoneurons that innervate inspiratory laryngeal or jaw muscles is usually biased to proximal dendrites (Nagase et al. 1997; Sun et al. 2002). There is also evidence that signals reaching medial or lateral dendrites of turtle hindlimb motoneurons can be selectively amplified by stimulation of different subsets of 5-HT axons (Delgado-Lezama et al. 1999). There are no descriptions of the distribution of NE synapses on alpha motoneurons (see Gladden et al. 2000, for a description based on gamma motoneurons). Thus, there is evidence that 5-HT synapses may be distributed non-uniformly on the

dendrites of motoneurons, but this is not a rule and the distribution of NE synapses is unknown.

The local perspective is based on the hypothesis that the distributions of 5-HT and NE synapses within their global distributions are not random. Instead, the distance between synapses based on the proximity to their nearest neighbour (adjacent 5-HT and 5-HT synapses, adjacent NE and NE synapses, or adjacent 5-HT and NE synapses) is designed to minimize or maximize interactions between the second messenger systems that are activated by 5-HT and NE. It has recently been found that induction of long term potentiation at a single synapse can reduce the threshold for induction of long term potentiation in neighbouring synapses, but only if the neighbouring synapses are less than 10 μm from the first synapse (Harvey & Svoboda, 2007). This cooperativity is mediated by the spread of active Ras, a second messenger (Harvey et al. 2008). These results suggest that activation of metabotropic receptors at a single NE or 5-HT synapse may increase the activity of second messengers in neighbouring regions and thereby reduce the level of activity in neighbouring 5-HT or NE synapses needed to modulate voltage-dependent channels. Thus, the modulation of voltage-dependent channels by 5-HT and NE would be a cooperative process that depends on the proximity of adjacent 5-HT and NE synapses. This type of interaction may represent another means by which monoamines regulate motoneuron input-output properties.

To determine how the local distributions of 5-HT and NE synapses may contribute to the regulation of motoneuron input-output properties, we compared the distance (measured by the volume of dendritic cytoplasm) between the nearest

neighbours of 5-HT and NE axon terminals to computer-generated distributions of synapses whose locations on the same dendritic tree were assigned randomly and independently.

1.8 Statement of Goals

1) To quantitatively describe the distribution of 5-HT and NE synapses on splenius motoneurons.

2) To characterize the relative proximity of adjacent pairs of NE-NE synapses, 5-HT-5-HT synapses, and NE-5-HT synapses on splenius motoneurons.

Chapter 2

Methods

2.1 Animal Preparation

Experiments were performed on 7 adult female felines weighing 3.3-3.9 kg. All experimental protocols were approved by the Queen's University Animal Care Committee. Animals were premedicated with a mixture of butorphanol (0.2 mg/kg; Torbugesic; Wyeth), acepromazine (0.05 mg/kg; Atravet; Ayerst Veterinary Laboratories) and glycopyrrolate (0.01 mg/kg; Sanoz) given subcutaneously 15-20 minutes prior to anesthesia induction. Ketamine (6.25 mg/kg; Vetalar; Bioniche Animal Health Canada Inc.) and midazolam (0.15 mg/kg; Sandoz) were administered intravenously to induce anesthesia. Deep anesthesia was maintained with supplementary doses of sodium pentobarbital (Ceva Santé Animale; 2.5-5 mg/kg) administered intravenously upon sudden increases in heart rate. This protocol maintained the heart rate between 140 to 165 beats per minute. Heart rate was continuously monitored with a V3395 TPR monitor (SurgiVet Inc., Waukesha Wisconsin USA). Rectal temperature was monitored using a YSI tele-thermometer system and maintained at 35-37°C with a heating blanket under negative feedback control. Normosol-R (Hospira Healthcare Corporation, Montreal) was administered intravenously at a constant rate (10 ml/kg/hour) to maintain body fluids.

A laminectomy extending from C1 to C4 was performed. The animals were subsequently secured in a stereotaxic frame (Transvertex, AB). The nerves supplying the

neck muscles, trapezius, biventer cervicis, complexus, and splenius neck were isolated and positioned on bipolar stimulating electrodes. The animals were paralyzed with gallamine triethiodide (Sigma; 2.5-5.0 mg/kg/hour) and artificially respired to maintain end tidal CO₂ between 3.7-4.5% as measured with a medical gas analyzer (LB-2 Beckman). A bilateral pneumothorax was performed to reduce respiratory related movements.

2.2 Motoneuron Identification and Intracellular Injections

Intracellular recordings were obtained with glass micropipettes broken to yield sharp tips ranging from 1.5-2 μm in diameter. The micropipettes were filled with 12% Neurobiotin (Vector Laboratories) in 0.5 M KCl and 0.10 M Trizma buffer (pH 8.2). Micropipette resistance varied from 10-17 M Ω . To prevent leakage of the positively charged Neurobiotin, a negative holding current of 5 nA was used while searching for motoneurons. Splenius motoneurons in C2 to C4 were antidromically identified by stimulating the C2 or C3 or C4 nerves that supply the splenius muscle.

Splenius motoneurons were stained by passing positive current pulses (450 ms at 2 Hz) of 6-10 nA for 3.5-5 min. The total charge delivered varied from 21.6-41.4 nA \cdot min. To minimize overlap of dendritic trees from adjacent motoneurons, each stained motoneuron was separated by a minimum of 3 mm. Because of this criterion and cardio-respiratory related moments that are common in the upper cervical segments and compromise the stability of intracellular penetrations, each experiment yielded one to six well-stained splenius motoneurons.

2.3 Perfusion and Tissue Processing

Several minutes prior to perfusion, heparin (25,000 IU) was intravenously administered and followed by a lethal dose of sodium pentobarbital. The animals were subsequently perfused with saline (1 liter), followed by 2 liters of fixative (4% paraformaldehyde in 0.1 M sodium phosphate buffer (pH 7.4)). The upper cervical spinal cord was removed and stored overnight (5-9 hours) in fixative. The tissue was subsequently stored in 15% sucrose in 0.1 M sodium phosphate buffer for 3 days.

Horizontal sections, 50 μm thick, of the spinal cord were cut using a freezing microtome (Leitz Wetzlar Germany; Model 44011). The sections were rinsed in 0.1 M sodium phosphate buffer and incubated in 1% sodium borohydride for 20 minutes to reduce tissue auto fluorescence. In pilot studies, the noradrenalin producing enzyme, dopamine- β -hydroxylase (DBH) was visualized using the same primary antibody (rabbit anti-DBH; 1:1000; polyclonal IGg, Biomol International LP) and protocol used by Gladden et al. (2000) and Hammar et al. (2004). Subsequent incubation with a secondary antibody (goat anti-rabbit; 1:1000; Molecular Probes) coupled with the Cy3 fluorochrome labeled terminals of DBH immunoreactive axons, similar to the results described by Gladden et al (200) and Hammer et al. (2004). However, if this protocol was preceded by an antigen retrieval technique that involved incubation with a sodium citrate buffer (pH 8.5) kept at 80°C for 30 minutes (Jiao et al. 1999), the intensity of the Cy3 fluorescence was greatly enhanced. DBH immunoreactive terminals now appeared as beads on a

clearly defined string and the overall density of terminals increased due to the improved visibility of smaller terminals. This antigen retrieval technique was therefore used in all experiments described in this study. Following the antigen retrieval protocol, sections were incubated overnight (17-18 hours) in 0.02 M Potassium phosphate buffer, with 2% natural goat serum (Vector Laboratories Inc.) to block non specific labeling, and 0.3% Triton X-100 (Fisher Scientific) to permeablize the tissue.

For visualization of the Neurobiotin filled motoneurons, sections were incubated with streptavidin conjugated to Alexa 488 (1:100; Invitrogen) for 3 hours with constant agitation. The sections were then mounted with Vectashield (Vector Laboratories) and coverslipped.

Serotonergic axon terminals were labeled after reconstruction of the motoneuron dendritic tree and identification of contacts with D β H axon terminals (see below). The slides with sections containing dendrites of the reconstructed neurons were soaked in 0.02 M potassium phosphate buffer and the sections were collected in serial order as they floated off the slides. Each section was incubated in 0.02 M potassium phosphate buffer with 6% natural goat serum and 0.9% Triton x-100, for 4 hours, followed by incubation with rat anti-5-HT (1:1000; polyclonal IGg, Biomol International LP) for 36 hours with constant agitation. This antibody was used in previous studies to visualize the distribution of 5-HT terminals on feline commissural interneurons and spinocerebellar neurons (Hammer and Maxwell, 2002; Hammer et al. 2004). Fluorescent labeling was achieved by incubation with goat anti-rat (1:200; Molecular Probes) coupled to the Alexa 488

fluorochrome, for 2.5 hours with constant agitation. Sections were remounted with Vectashield and coverslipped.

2.4 Reconstruction of Motoneuron Dendritic Trees

The trajectories of all dendrites on each section were drawn with the aid of an Olympus BX60 microscope and Lieca DMLB microscope equipped with either a Eutectic Neuron Tracing System (Eutectic Electronics Inc.) or NeuroLucida (version 5.05.40; MicroBrightField Inc.). For a full description of the reconstruction method, see Rose and Cushing (2004). The bandpass excitation and emission filters (Chroma Technology Corp., VT, USA) were selected to maximize fluorescence signals from Alexa 488 and Cy3, but minimize the possibility of visualizing Alexa 488 with the Cy3 filter set and vice versa. Despite the intense fluorescence generated by Alexa 488 in intracellularly stained motoneurons, their dendrites were not visible with the Cy3 filter set. Similarly, intensely stained Cy3 processes were not visible with the Alexa 488 filter set. The dendrites on each serial section were traced with a X40 dry objective, and converted into a series of XYZ coordinates with corresponding diameters. All processes were followed to their termination. This yielded a detailed three-dimensional description of the structure of the entire dendritic tree. The size of the data file was proportional to motoneuron size and was typically composed of 18,000 to 21,000 coordinates for motoneurons with a dendritic surface area of 550,000 μm^2 . Artifacts due to tissue

shrinkage and undulations in the surface were minimized using special purpose software provided by the Eutectic Neuron Reconstruction System.

2.5 Identification of Contacts

Contacts between dendrites and Alex 488 labeled 5-HT boutons or Cy3 labeled DBH boutons were visualized using a X60 dry objective on the Olympus BX60 microscope described above. Contacts were identified based on three criteria: 1) the bouton must be a round or elliptical swelling whose diameter was twice that of the adjacent collateral shaft, 2) there was no discernible gap between the swelling and the dendrite, and 3) both the swelling and the dendrite at the site of the potential contact were in the same focal plane. These criteria have been used in several previous studies (Fyffe, 1991; Rose et al. 1995; Alvarez et al. 1998; Carr et al. 1999, Lübke et al., 2000; Silver et al. 2003; Grande et al. 2005) and nearly 9 out of every 10 appositions meeting these criteria have been shown to correspond to synaptic contacts at the electron microscopic level (Fyffe, 1991; Markam et al. 1997; Alvarez et al. 1998; Lübke et al. 2000; Silver et al. 2003). This confirmation rate is independent of the type and location of synapses, including 5-HT synapses on spinal motoneurons. The locations of the 5-HT and NE contacts were added to the reconstruction of the dendritic tree with aid of NeuroLucida (version 5.05.40; MicroBrightField Inc.).

Chapter 3

Results

Data was collected from five splenius motoneurons stained in three animals. These motoneurons were selected based on the quality of their intracellular stain. All of the dendrites of these cells could be traced to their termination. Thus, the complete dendritic tree of each cell could be reconstructed. The characteristics of these cells are summarized in Table 3.1. Four of these cells had large dendritic trees, with a total dendritic length of 87,228-101,060 μm , and a total dendritic surface area of 539,354-604,769 μm^2 . The dendritic tree of the other cell, Sena 4-5, was smaller, having a total dendritic length of 67,466 μm , and a total dendritic surface area of 359,486 μm^2 . These cells, as a population, had 7-10 primary dendrites and somatic diameters ranging from 48 to 69 μm . The axonal diameter was measured at the narrowest point, the initial segment, and ranged from 2.0 to 4.5 μm . These measurements are typical of feline spinal motoneurons (Ulfhake & Kellerth 1984; Rose et al. 1985; Cameron et al. 1985; Cullheim et al. 1987; Kernell & Zwaagstra 1989; Fukunishi et al. 1999; Grande et al. 2005).

3.1 Distribution of Contacts

The neuropil in the vicinity of splenius motoneurons was densely innervated by NE and 5-HT axons. These axons followed a tortuous path that could be easily followed due to numerous en passant boutons that were arranged like beads on a string. Contacts between NE or 5-HT boutons and intracellularly stained dendrites were readily detected (Figure 3.1). There was one exception to this general rule. The high intensity of Alexa

Table 3.1 Morphological summary of all five reconstructed splenius motoneurons.

Cell name	Spinal segment	Initial segment diameter (μm)	Average somatic diameter (μm)	Number of primary dendrites	Total dendritic length (μm)	Total dendritic surface area (μm^2)
Sena 3-3	C3	4.5	48	7	101,060	566,088
Sena 4-4	C2	3.4	50	10	87,228	539,354
Sena 4-5	C3	2.0	57	9	67,466	359,486
Sena 4-8	C4	4.5	69	10	91,993	604,769
Sena 5-2	C3	3.4	53	8	88,735	575,313
Average	C3	3.6	55	9	87,296	529,002

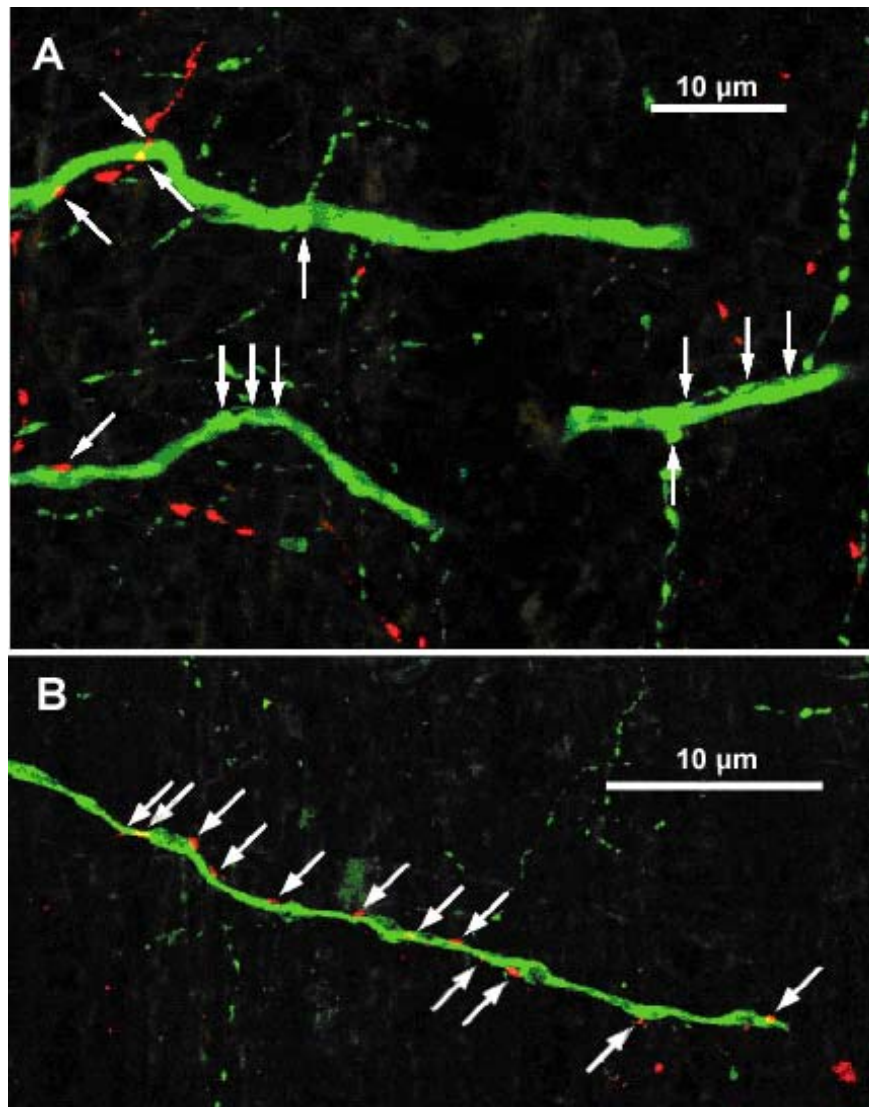


Figure 3.1 Confocal microscopy images of NE and 5-HT labeled boutons in contact with splenius motoneuron dendrites. The dendrites (large diameter processes) and 5-HT containing boutons (small strings of dots) are pseudo colored green, while NE boutons (small strings of dots) are pseudo colored red or yellow. Contacts between NE boutons and dendrites are indicated with angled arrows. 5-HT boutons contacting dendrites are identified by vertical arrows. Although confocal microscopy was not used to map the distribution of NE and 5-HT contacts on the dendrites of splenius motoneurons, the morphological details seen in these images were equally apparent using an epifluorescent microscopy equipped with a X60 dry objective and continuously adjusting the focus. Panels A and B are two separate regions of the dendritic tree belonging to Sena 3-3.

488 fluorescence in the somata and some large diameter dendrites caused by the intracellular stain obscured the labeling of 5-HT axons and contacts that were visualized with the same fluorochrome. Consequently, these regions were excluded from the analysis of 5-HT contacts. The regions on the proximal dendrites that were excluded varied for each cell. No regions were excluded on two cells, Sena 4-5 and Sena 5-2. Short zones, ranging from 12 to 61 μm from the soma, on 2 primary dendrites of Sena 3-3 and Sena 4-4 and 4 primary dendrites of Sena 4-8 were obscured. These zones represented 0.5%, 0.2% and 0.4% of the total dendritic surface area, respectively, for these cells. The distributions of all contacts between NE or 5-HT boutons and the dendrites of one of the intracellularly stained splenius motoneurons, Sena 3-3, are shown in Figure 3.2. Due to the large number of contacts, the distribution of NE and 5-HT contacts are shown separately on two copies of the same cell to avoid masking one set of contacts by the other set. The distribution of NE and 5-HT contacts was the same on all five cells. Contacts between NE or 5-HT boutons and dendrites of splenius motoneurons were found throughout the dendritic tree.

Table 3.2 summarizes the numbers of contacts per cell, and their respective densities according to dendritic surface area and dendritic length. The number of NE contacts per cell ranged from 1312 to 1508 for the four large cells. The small cell had 650 contacts, with an overall average of 1231 contacts per cell. The number of 5-HT contacts per cell was usually larger and ranged from 1400-2143 for the four large cells to 1249 for the smaller cell, with an overall average of 1586. This difference was not statistically significant. The density of NE contacts was relatively constant for the four large cells,

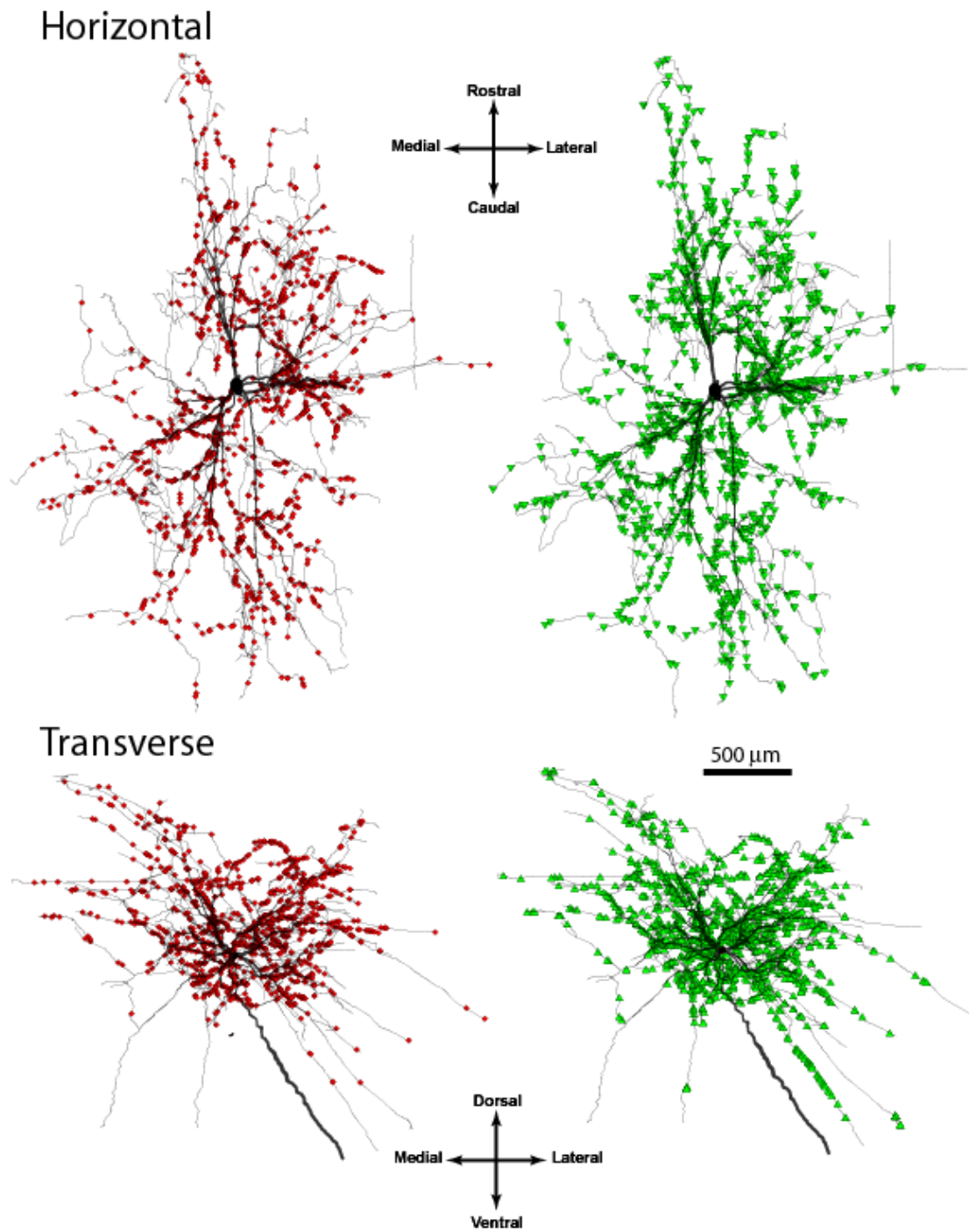


Figure 3.2 Distribution of NE and 5-HT contacts on Sena 3-3. The distribution of NE contacts (illustrated by filled red circles) and 5-HT contacts (represented by filled green triangles) are shown in both the horizontal (above) and transverse (below) view. There were 1340 NE contacts, and 1650 5-HT contacts shown throughout the dendritic tree.

Table 3.2 Summary of NE and 5-HT contacts for each motoneuron, reported as the absolute number and density with respect to dendritic surface area and dendritic length. Differences between the density of NE and 5-HT contacts were not significant (Wilcoxon test).

Cell Name	NE contacts	NE contact density (#/1000 μm^2)	NE contact density (#/100 μm)	5-HT contacts	5-HT contact density (#/1000 μm^2)	5-HT contact density (#/100 μm)
Sena 3-3	1340	2.37	1.33	1650	2.92	1.63
Sena 4-4	1312	2.43	1.50	2143	3.97	2.46
Sena 4-5	650	1.81	0.96	1249	3.47	1.85
Sena 4-8	1508	2.49	1.64	1400	2.32	1.52
Sena 5-1	1348	2.34	1.52	1489	2.59	1.68
Average	1232	2.23	1.39	1586	3.05	1.83

ranging from 2.34 to 2.49 contacts/1000 μm^2 of dendritic surface area and 1.33 to 1.64 contacts/1000 μm of dendritic length, respectively (Table 3.2, see also Figure 3.3). The smallest cell, which had a lower absolute number of contacts, also had a lower density of contacts, 1.81 contacts/1000 μm^2 of dendritic surface area and 0.96 contacts/1000 μm of dendritic length. The density of 5-HT contacts was more variable, ranging from 2.32 to 3.97 contacts/1000 μm^2 of dendritic surface area and 1.52 to 2.46 contacts/1000 μm of dendritic length. The density of contacts on the small cell was similar to the densities of contacts on the large cells.

There were no NE contacts on the cell bodies of any of the five reconstructed motoneurons. To confirm this observation, the cell bodies of five additional splenius motoneurons were analyzed. These cell bodies also had no NE contacts. The distribution of NE and 5-HT contacts on the initial segment of the axon of each reconstructed motoneuron was also examined. No NE or 5-HT contacts were found.

3.2 Center of Mass (COM) Analysis

To determine if there were subtle, but important, biases in the distribution of contacts that could not be detected by simple visual inspection, we also examined the distribution of contacts quantitatively. This analysis took advantage of a technique, called the centre of mass (COM), developed by Grande et al. (2005). This technique compares the distribution of observed contacts in the medial-lateral or rostral-caudal or ventral-dorsal axes to a computer generated distribution of contacts that is based on the assumption that contacts are distributed in proportion to dendritic surface area.

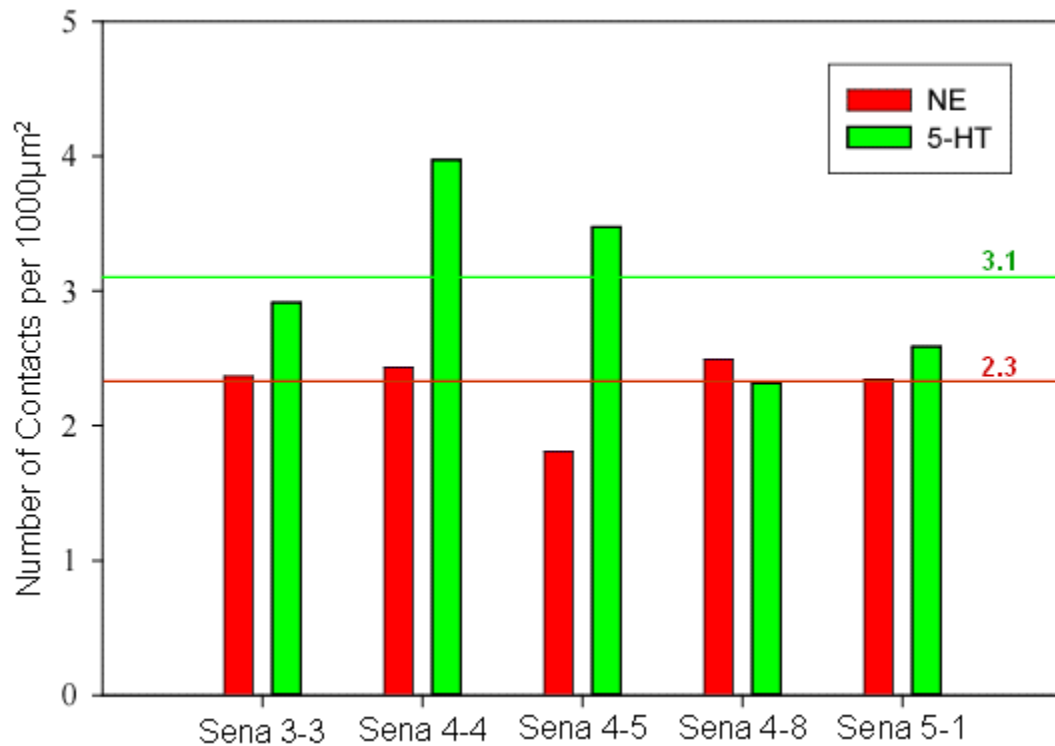


Figure 3.3 The density of NE and 5-HT contacts per 1000µm² of dendritic surface area for each cell. Below each pair of densities is the cell name, along with the total dendritic surface area for that cell. The average density for NE and 5-HT contacts across all cells is depicted with the red and green line respectively, with the numerical average placed above each line.

Application of the COM technique involves several steps which are explained pictorially in Figure 3.4. COM is defined as the mean XYZ coordinates of contacts on the dendritic tree, where the X-axis is aligned on the medial-lateral axis, the Y-axis is aligned on the rostral-caudal axis, and the Z-axis is aligned on the dorsal-ventral axis and the centre of the soma is assigned an XYZ coordinate of 0,0,0. The green star in Figure 3.4B indicates the COM of all 5-HT contacts on Sena 3-3. The position of this COM is compared to the COM of a uniformly distributed population of contacts as follows. First, the dendritic tree is divided into units of $28.6 \mu\text{m}^2$. This area corresponds to the dendritic area where one would expect to find one synapse based on two assumptions: 1) that synapses on splenius motoneurons are distributed in proportion to the dendritic surface area and 2) the density of synapses is $7/100 \mu\text{m}^2$. The latter assumption is consistent with estimates of the density of synapses on neck motoneurons based on ultrastructural observations (Rose and Neuber-Hess, 1991). Each unit of surface area is therefore assigned one synapse at an XYZ coordinate determined by the midpoint of the dendritic zone that corresponds to the unit of surface area. Figure 3.4C shows the positions of all 20,090 synapses assigned to Sena 3-3 using this algorithm and the COM of these synapses. The XYZ coordinates of a number of these synapses (equal to the number of observed contacts) are randomly selected and the COM is calculated based on these coordinates (Fig 3.4C2). This step is repeated 1000 times to generate the COM of 1000 randomly selected contacts where each contact is distributed according to the dendritic surface area (Fig 3.4C3). The cumulative histograms of the XYZ coordinates of the COMs compiled from all 1000 trials (Fig 3.4, C3-X-axis, C3-X-axis, C3-X-axis) provide a direct measure of the probability that the

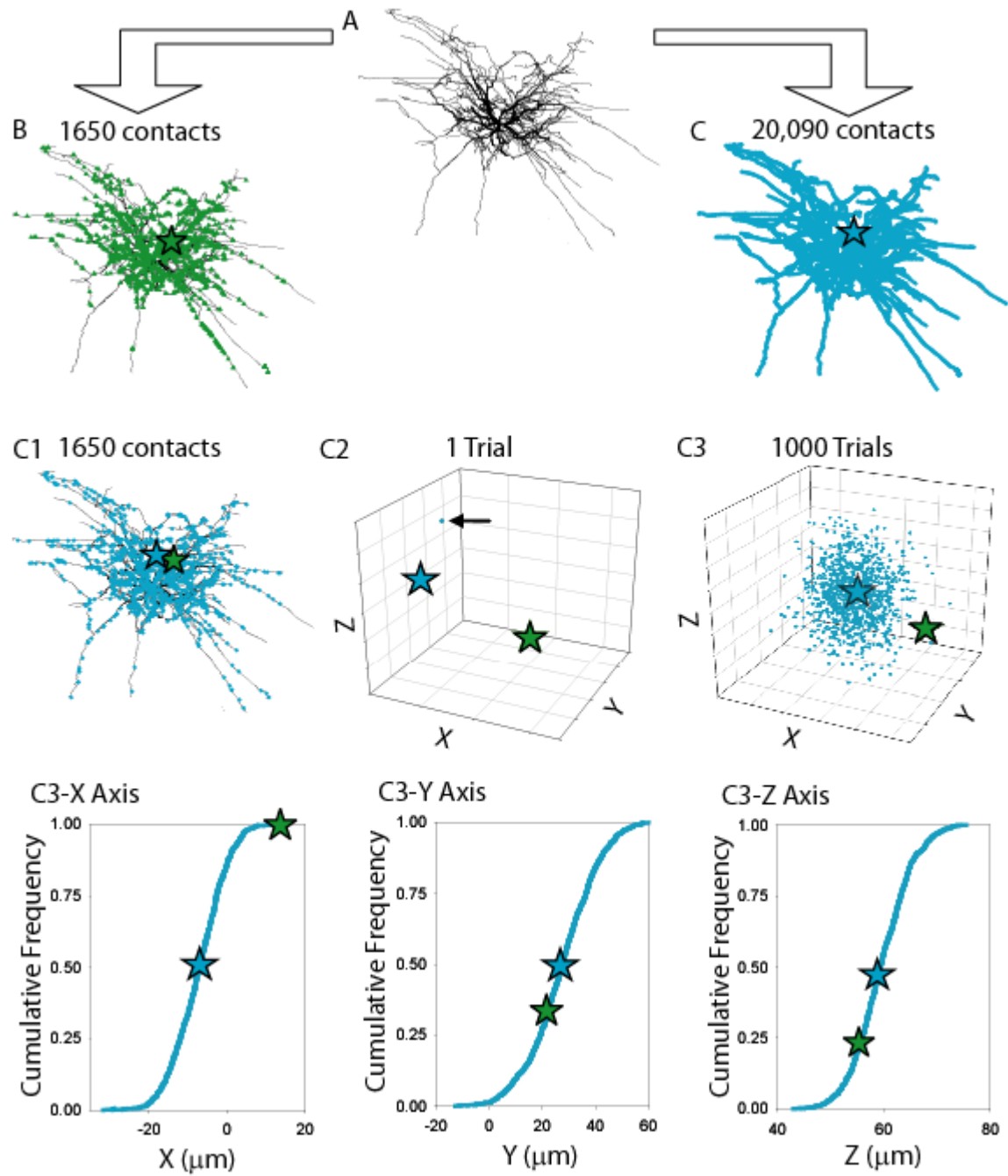


Figure 3.4 Description of the COM analysis. **A** Transverse view of the dendritic tree of Sena 3-3. **B** Distribution of 1650 5-HT contacts (filled green triangles), with the COM represented as a green star. **C** Computer-generated distribution of contacts ($n=20,090$, filled blue circles) based on a uniform density of 7 synapses/ $100 \mu\text{m}^2$. The blue star depicts the COM of all 20,090 contacts. **C1** Distribution of 1650 contacts (the same number as the observed 5-HT contacts) selected randomly from the 20,090 contacts shown in C. **C2** Three-dimensional scatter plot of the COM for the 1650 contacts in C1, shown as a single blue dot (marked by arrow), relative to the COMs for the observed contacts and 20,090 uniformly distributed contacts. The x-axis represents the medial-lateral direction, the y-axis represents the rostral-caudal direction, and the Z-axis represents the dorsal-ventral direction. **C3** Three-dimensional scatter plot of the COMs based on 1000 randomly selected groups of 1650 contacts. Each COM is shown as a single blue dot. **C3X-Z** Cumulative histograms of the X, Y, and Z coordinates of the COMs shown in C3. The position of the green star is determined by the XYZ coordinate of the observed COM. The probability that the observed COM is from the same population as the computer-generated COMs is equal to 2 times (equivalent of two tail test) the value of the Y coordinate of the observed COM if it is below 0.5, or 1 minus the value of the Y coordinate if the observed COM is above 0.5 (e.g. if the Y coordinate of the observed COM is 0.3 then $P = 2*0.3 = 0.6$, conversely if $Y = 0.99$ then $P = 2*(1 - 0.99) = 0.02$).

COM of the observed distribution of contacts is consistent (or not consistent) with the hypothesis that 5-HT (or NE) contacts are distributed according to the dendritic surface area.

The results of the COM analysis for all five cells are summarized for NE contacts in Table 3.3A, and for 5-HT contacts in Table 3.3B. With few exceptions, 5-HT and NE contacts were distributed in proportion to the dendritic surface area along the medial-lateral and rostral-caudal axes. In contrast, NE and 5-HT contacts were not uniformly distributed in the dorsal-ventral axis. The distribution of NE contacts was biased (i.e. more than would be expected based solely on dendritic surface area) towards dorsal dendrites of all five cells. In three of the five cells, more 5-HT contacts were found on ventral dendrites than expected based on their surface area. However, in absolute terms, the biases were small. The mean shifts in the NE and 5-HT COMs relative to the COM expected for a uniform distribution were only 31.2 μm and 15.8 μm respectively.

3.3 Proximal Versus Distal Gradients in the Distribution of 5-HT and NE Contacts

Figure 3.5 compares the numbers of 5-HT and NE contacts found on Sena 5-2 to the dendritic surface area as a function of the distance from the cell body. If 5-HT and NE contacts were distributed according to the dendritic surface area at different distances from the soma, the cumulative proportion of the surface area should predict (i.e. be identical to) the cumulative number of contacts. This did not occur. Instead, the cumulative numbers of 5-HT and NE contacts as a function of the dendritic surface area were shifted distally relative to the cumulative proportion of the surface area. The

Table 3.3A Summary of the X, Y, and Z coordinates of the observed COMs for NE contacts, relative to the COM based on a uniform density of 7 synapses/100 μm^2 . * indicates that the value of the observed COM was significantly different than the COMs based on a uniformly distributed set of contacts with the same number as the observed number of contacts

Cell	X-axis (+lateral)	Y-Axis (+rostral)	Z-Axis (+dorsal)
Sena 3-3	+44.6 P<0.001 *	-63.6 P<0.001 *	+46.7 P<0.001 *
Sena 4-4	-8.7 P>0.05	-50.5 P<0.001 *	+22.8 P<0.001 *
Sena 4-5	+2.2 P>0.05	+24.1 P>0.05	+29.1 P<0.001 *
Sena 4-8	+14.9 P<0.025 *	-14.0 P>0.05	+11.5 P<0.001 *
Sena 5-2	-3.2 P>0.05	+23.7 P>0.05	+49.4 P<0.001 *
Average	10.0 P>0.05	16.1 P>0.05	31.9 P<0.05 *

Table 3.3B Summary of the X, Y, and Z coordinates of the observed COMs for 5-HT contacts, relative to the COM based on a uniform density of 7 synapses/100 μm^2 .
 * indicates that the value of the observed COM was significantly different than the COMs based on a uniformly distributed set of contacts with the same number as the observed number of contacts.

Cell	X-axis (+lateral)	Y-Axis (+rostral)	Z-Axis (+dorsal)
Sena 3-3	+36.1 P<0.001 *	+5.0 P>0.05	-3.8 P>0.05
Sena 4-4	-4.1 P>0.05	-29.9 P<0.001 *	-42.6 P<0.001 *
Sena 4-5	+5.5 P>0.05	+42.3 P<0.025 *	-11.5 P<0.025 *
Sena 4-8	+24.7 P<0.001 *	-25.9 P>0.05	-16.5 P<0.001 *
Sena 5-2	+25.8 P<0.025 *	-25.1 P>0.05	-4.5 P>0.05
Average	17.4 P>0.05	-6.7 P>0.05	-15.8 P<0.05 *

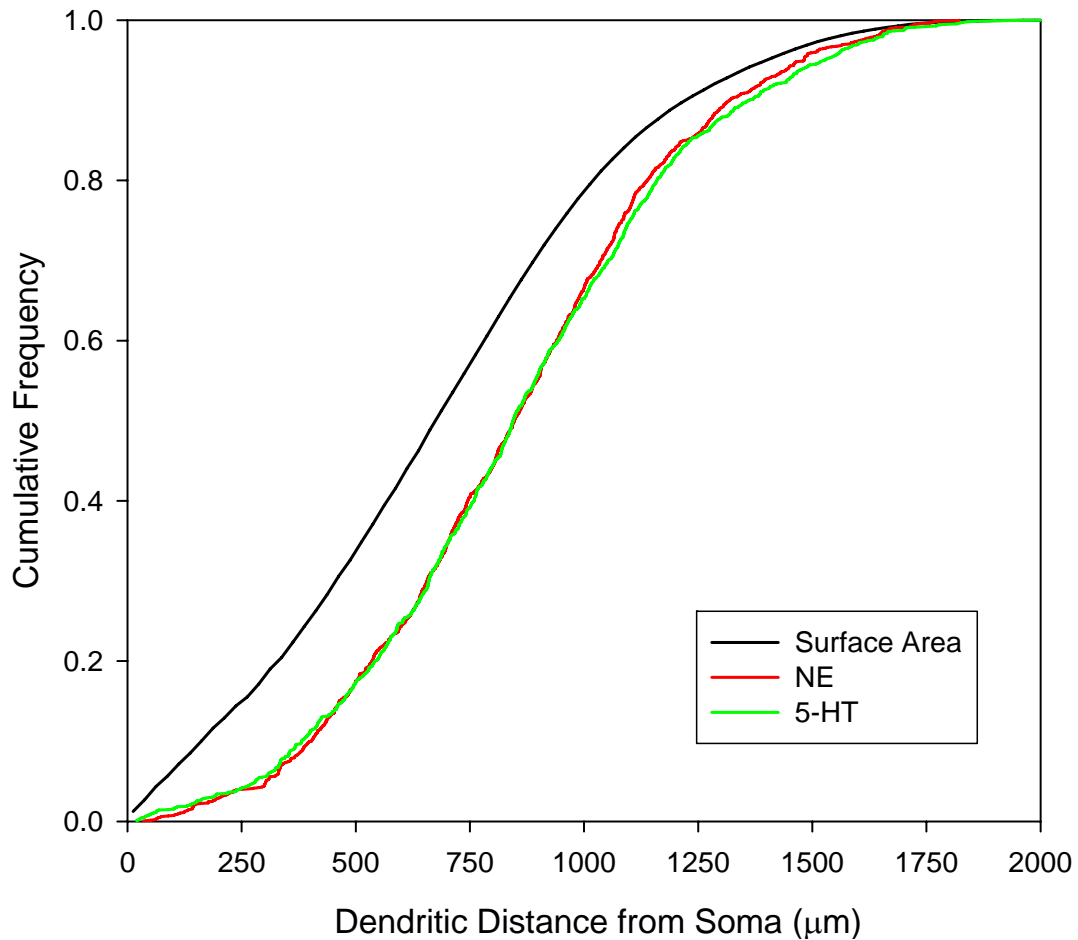


Figure 3.5 Dendritic distance from soma versus the cumulative frequency of dendritic surface area, and number of NE and 5-HT contacts, for Sena 5-2. The 0.5 frequency represents the median dendritic distance from the cell body. The median distances for NE and 5-HT contacts were located about 160 μm more distal than would be expected if these contacts were distributed in proportion to the surface area (and lay on top of the black line).

differences between the cumulative distributions of contacts versus surface area were significant ($P < 0.001$, two-sample Kolmogorov-Smirnov test). This shift was primarily due to a paucity of contacts in the first 250 μm . A summary of the NE data collected from all five cells is shown in Table 3.4A. NE contacts were consistently (five out of five cells) more distal than predicted by dendritic surface area alone. The magnitude of the distal shift varied from 53 to 167 μm , averaging 120 μm . In contrast, the results for 5-HT contacts were more variable, shown in Table 3.4B. 5-HT contacts were more distal than predicted by dendritic surface area alone in three of the five cells. The distribution of 5-HT contacts on one cell was consistent with the distribution of dendritic surface area and for the remaining cell, the distribution of 5-HT contacts were more proximal than predicted by dendritic surface area. Overall, 5-HT contacts were on average 64 μm more distal than would be predicted by surface area alone.

To better understand the factors that contributed to the relative paucity of NE and 5-HT contacts on proximal dendrites of most cells, the frequencies of NE and 5-HT contacts along dendrites of specific diameters were calculated, as summarized in Figure 3.6. On five of five cells, the numbers of NE or 5-HT contacts on dendrites less than 2 μm in diameter were significantly greater than would be expected if the contacts were distributed according to dendritic surface area. In contrast, the numbers of contacts on dendrites more than 5 μm in diameter were often less than expected based on the dendritic surface area available on these dendrites. This feature was also seen in all five cells.

Table 3.4A Proximal versus distal gradients in the distribution of NE contacts. * indicates that cumulative distributions of surface area versus the cumulative distributions of NE or 5-HT contacts were significantly different (two-sample Kolmogorov-Smirnov test) The average shift was analyzed with the Wilcoxon test, and significant shifts marked with an *.

Cell	Distal shift of median contact distance compared to median distance of dendritic surface area (μm)	Significance
Sena 3-3	127	P < 0.001 *
Sena 4-4	94	P < 0.001 *
Sena 4-5	53	P < 0.001 *
Sena 4-8	167	P < 0.001 *
Sena 5-2	159	P < 0.001 *
Average	120	P < 0.05 *

Table 3.4B Proximal versus distal gradients in the distribution of 5-HT contacts. * indicates that cumulative distributions of surface area versus the cumulative distributions of NE or 5-HT contacts were significantly different (two-sample Kolmogorov-Smirnov test) The average shift was analyzed with the Wilcoxon test, and significant shifts marked with an *.

Cell	Distal shift of median contact distance compared to median distance of dendritic surface area (μm)	Significance
Sena 3-3	95	P < 0.001 *
Sena 4-4	-32	P < 0.025 *
Sena 4-5	-24	P > 0.05
Sena 4-8	125	P < 0.001 *
Sena 5-2	158	P < 0.001 *
Average	64	P > 0.05

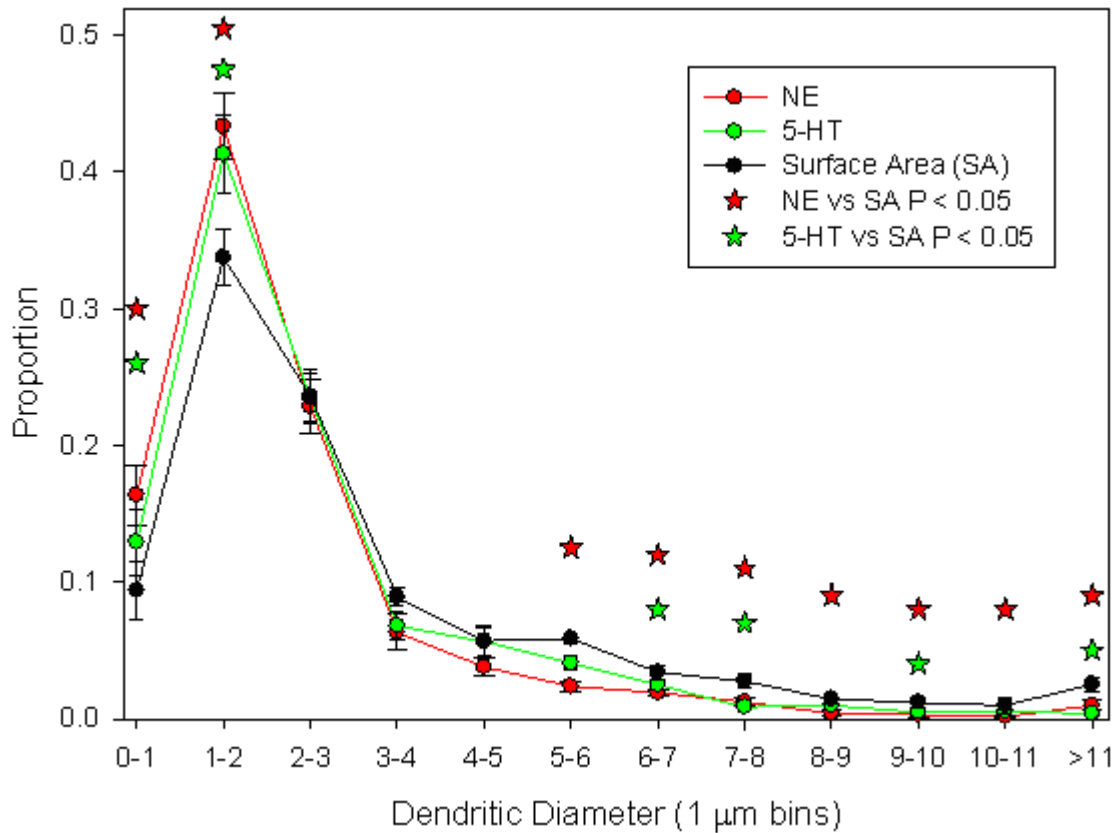


Figure 3.6 The proportion of contacts and dendritic surface area as a function of dendritic diameter. Data from all five cells were combined. The error bars indicate the standard error. Data related to NE and 5-HT contacts are shown in red and green, respectively. The stars indicate dendrites with a significantly different frequency of NE or 5-HT contacts compared to the frequency predicted by the dendritic surface area ($P < 0.05$, Wilcoxon test).

To determine if the bias of NE and 5-HT contacts to small diameter dendrites accounts for the bias of NE and 5-HT contacts to distal dendrites, the algorithm that generated a uniform distribution of contacts was modified. The new algorithm included a weighting factor for synaptic density that depended on dendritic diameter. Thus, synaptic density was uniform on dendrites within a given diameter range (e.g. 4.1 to 5.0 μm), but higher or lower on dendrites in other diameter ranges. The exact values of the weighting factors were determined separately for each cell (i.e. they were not based on the average results shown in Figure 7). The effect of applying a set of diameter-related weighting factors, specific for Sena 5-2, is shown Figure 3.7. For this cell, the bias of 5-HT or NE contacts to small diameter dendrites accounted for approximately 50% of the distal shift in the distribution of NE and 5-HT contacts relative to the distribution of contacts predicted by a uniform distribution. The effect of diameter weighting on the generated distribution of NE contacts is summarized in Table 3.5A. In four of the five cells the diameter-weighted distribution was a closer match to the observed distribution than a distribution based solely on surface area. In these four cells 43-76% of the distal shift in the observed distribution was accounted for by the bias of NE contacts to small diameter dendrites. However, the diameter-weighted distribution for Sena 4-5 was a poorer estimate of the observed distribution than surface area. Overall the locations of computer generated contacts that were weighted according to the dendritic diameter were no better than the locations of contacts based on surface area only, as a means of predicting the proximal to distal distribution of the observed NE contacts. Thus, although the bias to

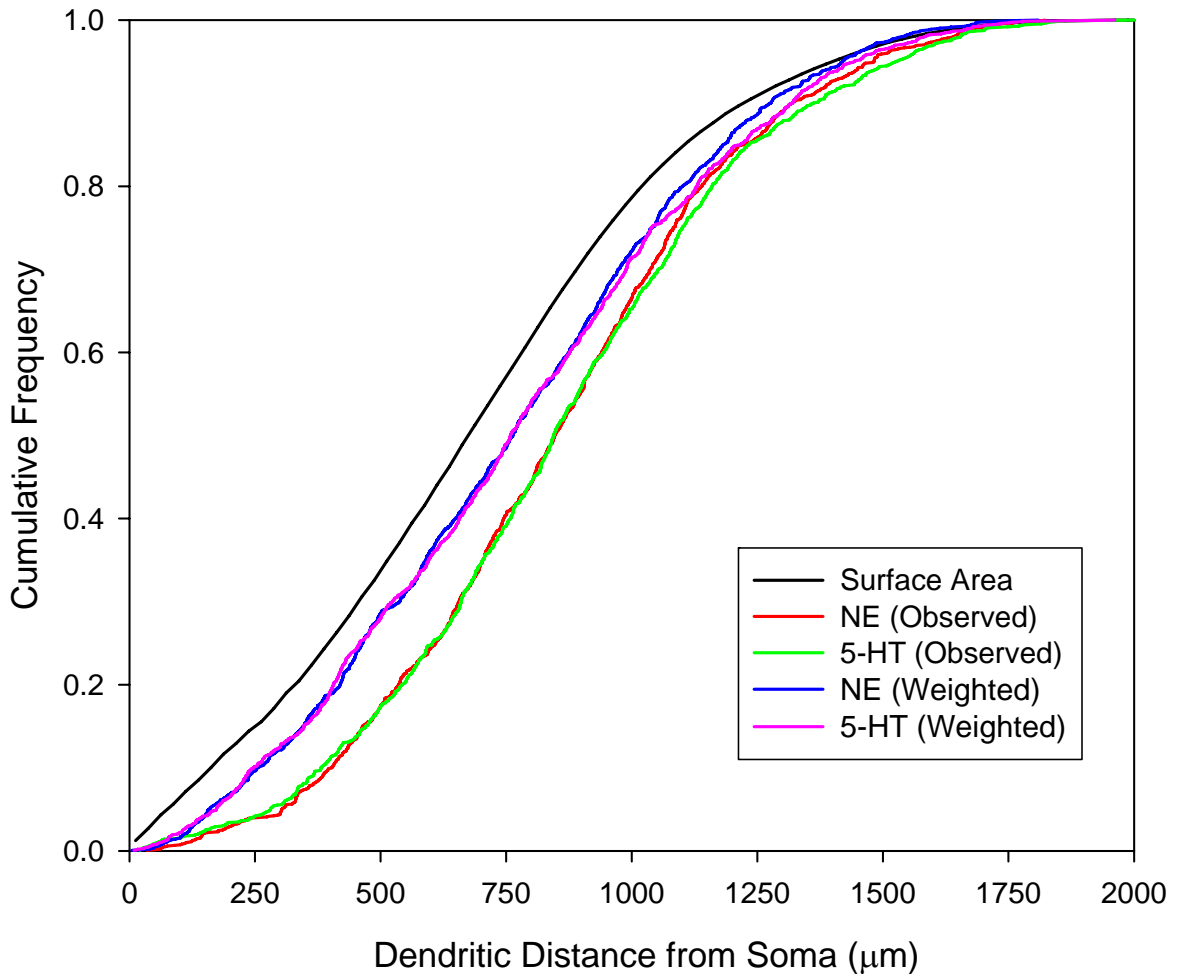


Figure 3.7 Comparison of the dendritic distances from soma to observed NE and 5-HT contacts on Sena 5-2 and NE and 5-HT contacts from a computer generated distributions that were diameter-weighted. The distribution of the observed NE and 5-HT contacts show a distal shift. The magnitude of this shift is reduced if the observed contacts are compared to a computer generated set of contacts where the density of contacts is uniform on dendrites within a given 1.0 μm diameter range (e.g. 4.1 to 5.0 μm), but higher or lower on dendrites in other diameter ranges. The values of these densities matched the densities of the observed NE and 5-HT contacts on the dendrites of Sena 5-2 subdivided as shown in Figure 3.6.

Table 3.5A Effect of the bias to small diameter dendrites by NE contacts on the proximal to distal gradient of the distribution of NE contacts. Negative numbers represent cases where the locations of computer generated contacts that were weighted according to the dendritic diameter were a poorer estimate of the locations of the observed NE contacts than the dendritic surface area. * indicates that the cumulative distribution of the locations of the computer generated contacts, weighted according to the dendritic diameter, versus the cumulative distribution of the locations of the observed NE contacts were significantly different (two-sample Kolmogorov-Smirnov test) The average shift was analyzed with the Wilcoxon test, was not significant.

Cell	Percentage of distal shift in the location of the observed contacts (relative to their location predicted by dendritic surface) that was accounted for by the bias to small diameter dendrites (based on a comparison of the median locations)	Probability
Sena3-3	76%	P<0.05*
Sena4-4	44%	P<0.05*
Sena4-5	-8%	P<0.05*
Sena4-8	43%	P<0.05*
Sena5-2	50%	P<0.05*
Average	41%	P>0.05

small diameter dendrites may explain part of the relative paucity of NE contacts on proximal dendrites, other factors must also contribute to the preference to distal dendrites.

Table 3.5B summarizes the effect of weighting the distributions of the computer generated contacts according to the observed preference of 5-HT contacts for small diameter dendrites. For all three of the cells which displayed a bias of the observed 5-HT contacts to distal dendrites, the diameter-weighted distribution was a better estimate of the observed distribution than the distribution that was based on surface area only. For Sena 3-3, the cumulative distribution of the locations of the observed contacts was not significantly different from the cumulative distribution of the locations of a set of computer generated contacts that were weighted according to the dendritic diameter. However, for the other two cells, the predicted proximal to distal location of the 5-HT contacts was worse based on the diameter-weighted distribution compared to the prediction based on surface only. Thus, for the population of cells as a whole, the diameter-weighted distribution was not significantly better than surface area as an estimate the distribution of the observed 5-HT contacts with respect to distance from the cell body.

3.4 Distribution of NE and 5-HT Contacts Relative to Other NE and 5-HT Contacts

3.4.1 5-HT to 5-HT Contacts and NE to NE Contacts

The distribution of NE contacts relative to other NE contacts, or 5-HT contacts relative to other 5-HT contacts, was determined for each NE and 5-HT contact by measuring the cytoplasmic volume between neighbouring contacts on the dendritic tree.

Table 3.5B Effect of the bias to small diameter dendrites by 5-HT contacts on the proximal to distal gradient of the distribution of 5-HT contacts. Negative numbers represent cases where the locations of computer generated contacts that were weighted according to the dendritic diameter were a poorer estimate of the locations of the observed 5-HT contacts than the dendritic surface area. * indicates that the cumulative distribution of the locations of the computer generated contacts, weighted according to the dendritic diameter, versus the cumulative distribution of the locations of the observed 5-HT contacts were significantly different (two-sample Kolmogorov-Smirnov test) The average shift, analyzed with the Wilcoxon test, was not significant.

Cell	Percentage of distal shift in the location of the observed contacts (relative to their location predicted by dendritic surface) that was accounted for by the bias to small diameter dendrites (based on a comparison of the median locations)	Probability
Sena3-3	92%	P>0.05
Sena4-4	-50%	P<0.05*
Sena4-5	-328%	P<0.05*
Sena4-8	88%	P<0.05*
Sena5-2	51%	P<0.05*
Average	-31%	P>0.05

This process is illustrated in Figure 3.8. Each NE (or 5-HT) contact was used as a ‘reference’ contact. A search for all immediately adjacent contacts, regardless of whether they were on the same dendritic branch as the ‘reference’ contact or on side branches, was conducted from this point. The contact with the least cytoplasmic volume between it and the ‘reference’ contact was defined as the nearest neighbour. These steps were repeated for all contacts.

The dendritic volume between pairs of 5-HT or NE contacts, defined as nearest neighbours, was compared to the dendritic volume that separated nearest neighbour pairs of a computer generated set of contacts (Fig. 3.8C). These contacts were distributed on the dendritic tree using the diameter-weighted algorithm described above. This distribution was designed to mimic the observed number of NE and 5-HT contacts and their bias to small diameter dendrites. However, there was one critical difference between the computer generated distribution of contacts and the distribution of the observed contacts. The computer generated contacts were selected *randomly* from a large set (typically close to 20,000, Fig. 3.8C1) of uniformly distributed contacts (weighted according to the dendritic diameter). As a consequence of this selection process, this distribution provided a measure of the nearest neighbour volumes between a set of contacts where the position of each contact did not depend on the position of its neighbour (Fig 3.8C2 and C3; note: by matching the densities of the computer generated contacts to the densities of the observed contacts and using the same dendritic tree for both sets of contacts, differences in the proximity of neighbouring synapses due to differences in dendritic diameter are excluded).

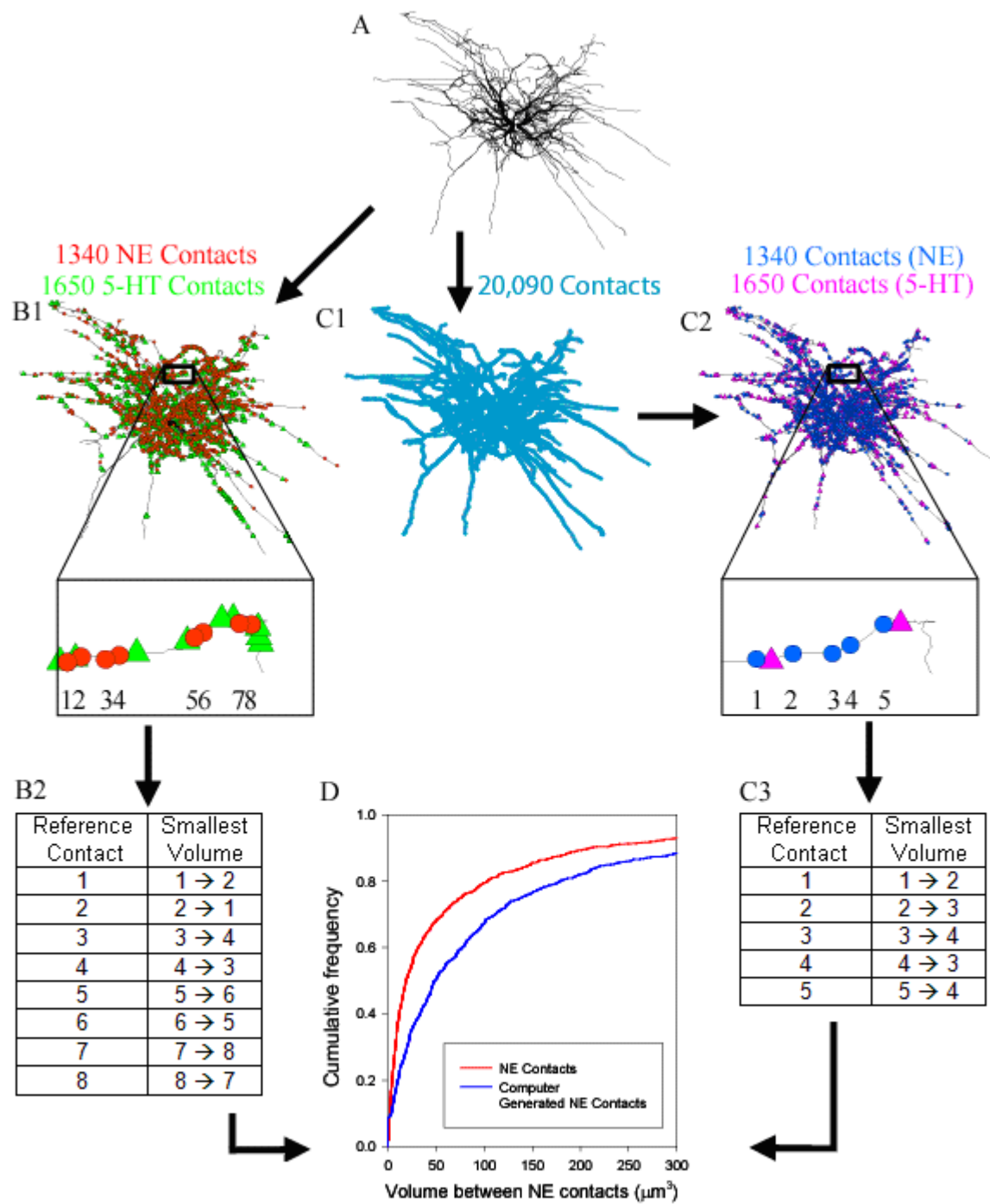


Figure 3.8 Description of nearest neighbor analysis. **A** Transverse view of the dendritic tree of Sena 3-3. **B1** Distribution of 1340 NE (filled red circles) and 1650 5-HT (filled green triangles) contacts. The inset shows a higher magnification view on one dendritic branch. Each NE contact was assigned a number. **B2** Identification of nearest neighbors of NE contacts. **C1** Computer-generated distribution of contacts (n=20,090, filled blue circles) based on a uniform density of 7 synapses/100 μm^2 . **C2** Distribution of 1340 NE contacts and 1650 5-HT contacts (the same number as the observed contacts) selected from the 20,090 contacts shown in C. This selection process took into account the dependency of contact density on dendritic diameter (cf. Figure 3.6). The inset shows a higher magnification view on one dendritic branch. Each computer generated NE contact was assigned a number. **C3** Identification of nearest neighbors for computer generated NE contacts. **D** Cumulative histograms of the dendritic volume between nearest neighbour pairs of the observed NE contacts and between nearest neighbour pairs of computer generated contacts.

Figure 3.9 compares the cumulative histograms of the volumes between nearest neighbours composed of pairs of observed NE and 5-HT contacts to nearest neighbours composed of computer generated contacts on Sena 5-2. There is a large rightward shift in the cumulative histogram of the volumes between the nearest neighbours composed of computer generated contacts. This indicates that the pairs of contacts in the observed distribution are much closer together than would be expected if the locations NE or 5-HT contacts were independent of the positions of their adjacent contacts. Table 3.6A and 3.6B are summaries of the volumes between nearest neighbours composed of pairs of NE and 5-HT contacts, respectively, to the volumes between nearest neighbours composed of computer generated contacts for all five cells. For all five cells, the median volume between nearest neighbour pairs of NE or 5-HT contacts was less than the median volume between nearest neighbour pairs of computer generated contacts. This difference was due to a marked leftward shift in the cumulative distribution of the nearest neighbour volumes of the observed NE or 5-HT contacts relative to the cumulative distribution of the nearest neighbour volumes of the computer generated contacts (Figure 3.9; the difference between the observed NE or 5-HT nearest neighbour volume distributions and the nearest neighbour volume distributions based on the computer generated contacts was significant for all cells, $P < 0.001$, two-sample Kolmogorov-Smirnov test). The average of the median volumes between nearest neighbour pairs of NE and 5-HT was $19 \mu\text{m}^3$ and $14.5 \mu\text{m}^3$, respectively. These volumes were one third of the average of the median volumes between nearest neighbour pairs of computer generated contacts, $57.6 \mu\text{m}^3$ and $47.1 \mu\text{m}^3$, respectively (Table 3.6A and 3.6B). Thus, the proximity of neighbouring pairs

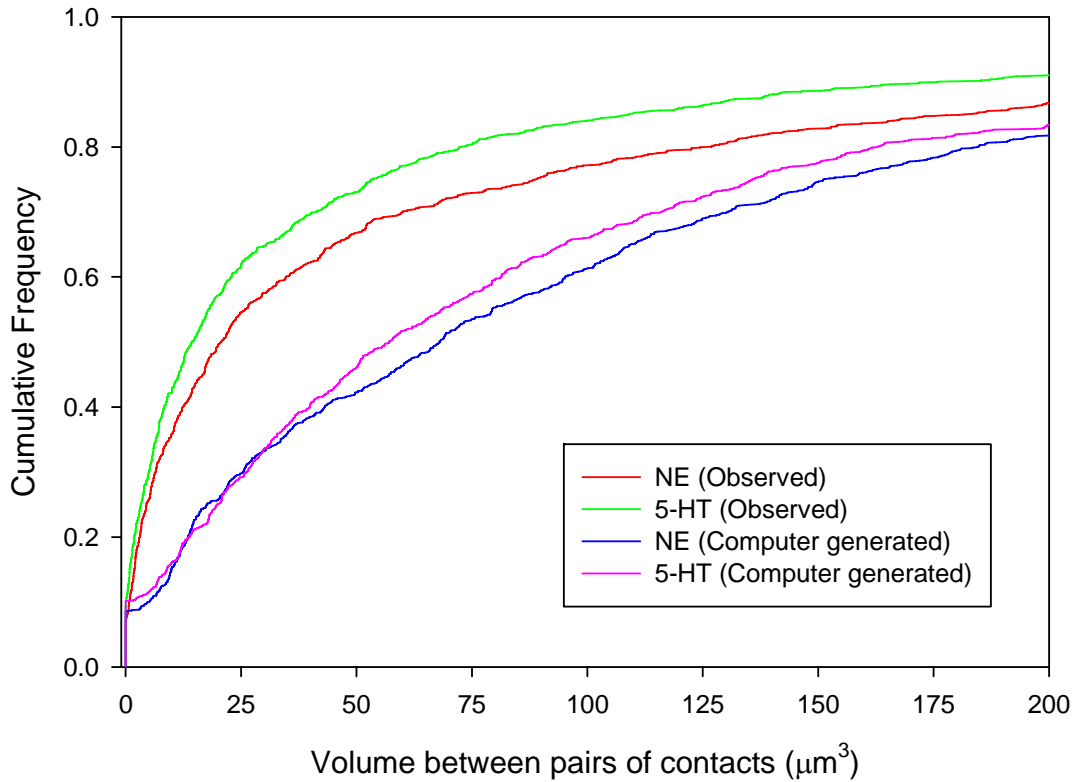


Figure 3.9 Comparison of the volume between nearest neighbour pairs of observed NE and 5-HT contacts on Sena 5-2 and nearest neighbour pairs of NE and 5-HT contacts from computer generated distributions that were diameter-weighted (cf. Figure 3.6). The differences between the cumulative histograms based on the observed contacts and the computer generated contacts were significant ($P < 0.001$) for both NE and 5-HT (two-sample Kolmogorov-Smirnov test).

Table 3.6A Median volume between nearest neighbors of pairs of observed NE contacts and diameter-weighted, computer generated, contacts. ^{*1} marks significant differences between the nearest-neighbor analysis of the diameter-weighted, computer generated, distributions of contacts, and the distribution of observed contacts (two-sample Kolmogorov-Smirnov test, P < 0.001). The average difference in volume between the populations was found to be significant, and marked with a ^{*2} (Wilcoxon test, P < 0.05).

	Based on the observed distributions (μm^3)	Based on a computer generated diameter-weighted distribution (μm^3)
Sena 3-3	18.6	58.4 ^{*1}
Sena 4-4	21.0	44.4 ^{*1}
Sena 4-5	18.3	70.1 ^{*1}
Sena 4-8	16.2	46.8 ^{*1}
Sena 5-2	20.7	68.1 ^{*1}
Average	19.0	57.6 ^{*2}

Table 3.6B Median volume between nearest neighbors of pairs of observed 5-HT contacts and diameter-weighted computer generated, contacts. ^{*1} marks significant differences between the nearest-neighbor analysis of the diameter-weighted, computer generated, distributions of contacts, and the distribution of observed contacts (two-sample Kolmogorov-Smirnov test, P < 0.001). The average difference in volume between the populations was found to be significant, and marked with a ^{*2} (Wilcoxon test, P < 0.05).

	Based on the observed distributions (μm^3)	Based on a computer generated diameter-weighted distribution (μm^3)
Sena 3-3	18.9	49.7 ^{*1}
Sena 4-4	11.0	43.6 ^{*1}
Sena 4-5	12.2	41.2 ^{*1}
Sena 4-8	16.1	44.0 ^{*1}
Sena 5-2	14.3	57.1 ^{*1}
Average	14.5	47.1 ^{*2}

of NE or 5-HT contacts is not random. Instead, the distance between pairs of NE or 5-HT contacts is purposefully small.

3.4.2 NE to 5-HT Contacts and 5-HT to NE Contacts

The distribution of NE contacts relative to 5-HT contacts, or 5-HT contacts relative to NE contacts, was determined for each NE and 5-HT contact by measuring the cytoplasmic volume between neighbouring contacts on the dendritic tree. This process is the same as previously described for determining the volume between nearest-neighbour pairs of NE or 5-HT contacts, as summarized in Figure 3.8. Figure 3.10 shows a cumulative histogram of volumes between NE contacts and the nearest 5-HT contact for Sena 5-2. The same cell was also analyzed using 5-HT contacts as the reference, and determining the volume to the nearest NE contact. These cumulative distributions were compared to cumulative distributions of the volume between nearest-neighbour contacts from computer generated sets of contacts, distributed on the dendritic tree using the diameter-weighted algorithm described above. The cumulative distributions of the nearest-neighbour volumes between the computer generated contacts were shifted to the left of the cumulative distributions of the nearest-neighbour volumes between the observed contacts. This indicates that the volumes between nearest-neighbour NE and 5-HT contacts were much farther apart than would be predicted based on the assumption that the positions of 5-HT contacts and NE contacts are independent.

The differences between the nearest-neighbour volume of the observed contacts and the computer generated contacts are summarized in Table 3.7A and 3.7B. Using NE

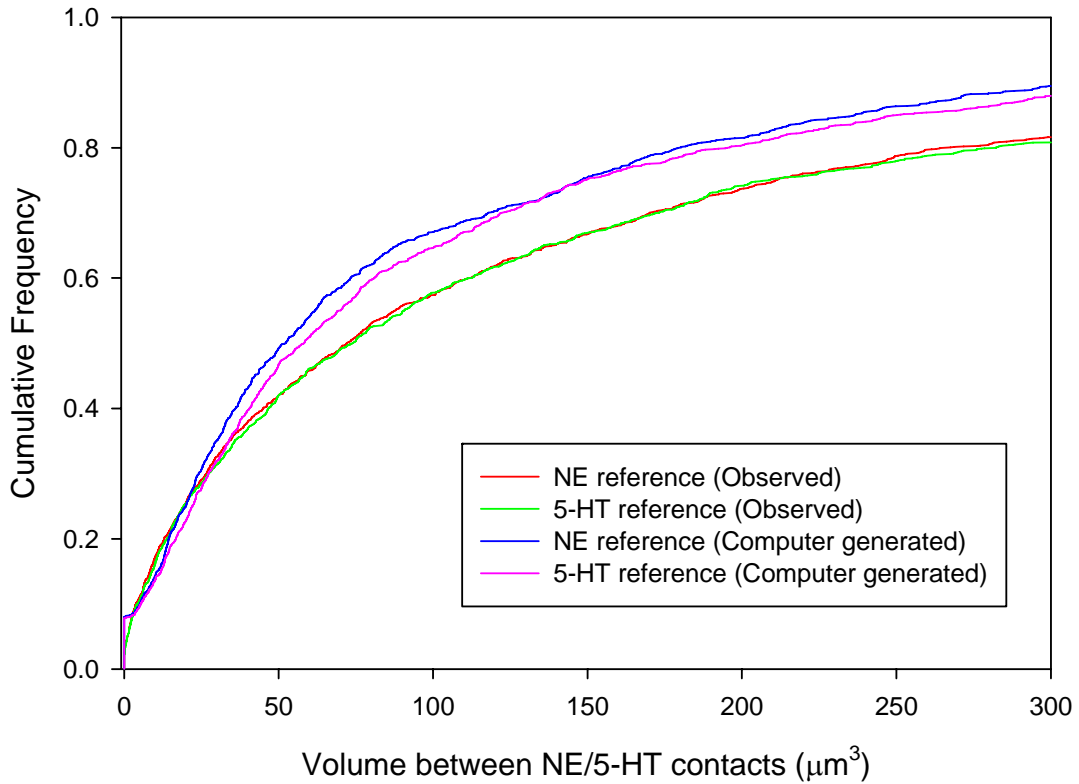


Figure 3.10 Comparison of the volume between nearest neighbours of observed NE/5-HT contacts on Sena 5-2 and nearest neighbours of NE/5-HT contacts from computer generated distributions that were diameter-weighted (cf. Figure 3.6). The differences between the cumulative histograms based on the observed contacts and the computer generated contacts were significant ($P < 0.001$) for both NE and 5-HT (two-sample Kolmogorov-Smirnov test).

Table 3.7A Median volume between nearest neighbors of pairs of NE/5-HT contacts, and contacts selected from two, independent, computer generated, sets of contacts, distributed using a diameter-weighted algorithm. NE contacts were used as the reference contact. ^{*1} marks significant differences between the diameter-weighted, computer-generated distribution of volumes, and the distribution of volumes based on observed contacts (two-sample Kolmogorov-Smirnov test, P < 0.001). The average difference in volume was significant and marked with a ^{*2} (Wilcoxon test, P < 0.05).

	Based on the observed distributions (μm^3)	Based on computer generated diameter-weighted distribution (μm^3)
Sena 3-3	53.2	45.0 ^{*1}
Sena 4-4	62.3	42.2 ^{*1}
Sena 4-5	56.0	43.9 ^{*1}
Sena 4-8	78.9	46.5 ^{*1}
Sena 5-2	72.1	52.5 ^{*1}
Average	64.5	46.0 ^{*2}

Table 3.7B Median volume between nearest neighbors of pairs of NE/5-HT contacts, and contacts selected from two, independent, computer generated, sets of contacts, distributed using a diameter-weighted algorithm. 5-HT contacts were used as the reference contact. ^{*1} marks significant differences between the diameter-weighted computer-generated distribution of volumes, and the distribution of volumes based on observed contacts (two-sample Kolmogorov-Smirnov test, P < 0.001). The average difference in volume was significant and marked with a ^{*2} (Wilcoxon test, P < 0.05).

	Based on the observed distributions (μm^3)	Based on computer generated diameter-weighted distribution (μm^3)
Sena 3-3	76.1	58.7 ^{*1}
Sena 4-4	106.6	74.1 ^{*1}
Sena 4-5	123.4	86.2 ^{*1}
Sena 4-8	77.9	41.6 ^{*1}
Sena 5-2	73.8	58.3 ^{*1}
Average	91.6	63.8 ^{*2}

as the reference, in Table 3.7A, each of the five cells had a median volume between the nearest neighbours of the observed contacts that was greater than the median volume between the nearest-neighbours of the computer generated contacts. The difference in the median volume was significant for all five cells (two-sample Kolmogorov-Smirnov test, $P < 0.001$). The average of the median volume between the nearest-neighbours of the observed contacts was $64.5 \mu\text{m}^3$. This value was significantly higher than the average of the median volume between the nearest-neighbour of the computer generated contacts, $46.0 \mu\text{m}^3$ (Wilcoxon test, $P < 0.05$). As a population of cells, the median volume between nearest neighbours of the observed contacts was significantly greater than those for the computer generated distribution (Wilcoxon, $P < 0.05$).

When 5-HT is used as a reference, in Table 3.7B, the volume between observed contacts is greater than the computer generated contacts in all five cells. The difference in the median volume was highly significant for each cell (two-sample Kolmogorov-Smirnov test, $P < 0.001$). As a population of cells, the median volume between nearest neighbours of the observed contacts was significantly greater than those for the computer generated distribution, when using 5-HT as the reference contact. (Wilcoxon, $P < 0.05$). The average of the median volumes between nearest neighbours of observed NE to 5-HT contacts was $64.5 \mu\text{m}^3$ and $91.6 \mu\text{m}^3$, using NE or 5-HT as a reference respectively. The average of the median volumes between nearest neighbours of computer generated NE to 5-HT contacts was $46.0 \mu\text{m}^3$ and $63.8 \mu\text{m}^3$, using NE or 5-HT as a reference respectively. Thus, the proximity of neighbouring 5-HT contacts to NE contacts, regardless of which

contact is used as a reference, is not determined by chance. Instead, the volume between NE and 5-HT contacts is purposefully large.

Chapter 4

Discussion

Ionotropic inputs to motoneurons are amplified by the monoamines NE and 5-HT. These monoamines amplify synaptic currents through the modulation of voltage dependent/independent channels located throughout the dendritic tree, soma, and initial segment (Hounsgaard & Kiehn, 1985; 1989; Wallén et al. 1989a; 1989b; Fung & Barnes, 1987; Berger, 1995; Talley & Bayliss, 2000; Hayar et al. 2001; Dai et al. 2002; Perrier et al 2002; 2003; Sirois et al. 2002; Franceschetti et al. 2003, Heckman et al. 2003, Fedirchuk & Dai, 2004; Gilmore & Fedirchuk, 2004; Grunnet et al. 2004; Harvey et al. 2006a; 2006b). Synaptic inputs, such as those from the vestibular system onto splenius motoneurons, are localized to specific regions of the dendritic tree (Grande et al. 2005). Since some synaptic inputs are located along specific regions of the dendritic trees of motoneurons, the dendritic distribution of neuromodulatory inputs plays a crucial role in the amplification of these inputs. The distribution of 5-HT contacts along motoneurons has been described for jaw, hindlimb, and laryngeal motoneurons (Nagase et al. 1997; Alvarez et al. 1998; Sun et al. 2002). However, these distributions vary largely between motoneuron types. This prevented the extrapolation of known distributions of 5-HT contacts to neck motoneurons. The distribution of NE contacts along alpha motoneurons has not been characterized for any alpha motoneuron.

The first goal of this investigation was to determine the distribution of NE and 5-HT input along the dendritic trees of feline splenius motoneurons. We found that there are no regions along the dendritic tree without input from NE and 5-HT. There were,

however, regions of high and low density of NE and 5-HT contacts. Regions of high and low density of NE or 5-HT contacts will amplify synaptic inputs which are also located in those regions, more than inputs in other regions.

The second goal of this study was to determine if the distribution of NE and 5-HT serves to minimize or maximize, the relative proximity of the contacts, and thus minimize or maximize the degree of interaction between contacts. Analysis of the relative proximity between contacts uncovered multiple trends in their arrangements. Pairs of NE contacts were preferentially located in close proximity, as well as pairs of 5-HT contacts. The close proximity of these contacts increases the probability of local interactions between these inputs. However, the cytosolic volume between NE contacts and their nearest 5-HT neighbour, or vice versa, is significantly higher than if the two populations were distributed independently. This suggests that the locations of NE and 5-HT contacts are distributed to minimize interactions between these inputs, during co-activation.

4.1 Methodological Considerations

4.1.1 Sample Size

All of the results reported in this study, except those regarding somatic innervation, were based on five motoneurons. Although this sample size is typical in studies of this kind (Rose et al. 1995; Burke & Glenn, 1996; Alvarez et al. 1998; Grande et al. 2005), the question remains whether these five motoneurons are representative of the population as a whole. There are several reasons we believe these five cells were representative of the splenius motoneurons population.

Firstly, the morphological characteristics of the five cells of this study were within the ranges of a much larger pool of splenius motoneurons that have previously been described (Keirstead & Rose, 1983; Rose et al. 1985; Grande et al. 2005).

Secondly, the motoneurons selected for analysis were chosen solely based on the quality of their intracellular staining. The quality of the intracellular staining was determined by a combination of two main factors: the quality of the somatic impalement of the motoneuron, and the degree of respiratory and cardiac related movements during the injection of Neurobiotin (See Methods). However, these selection criteria are slightly biased towards motoneurons with larger somata, since they provide a larger and more stable target for the electrode. Therefore, while the sizes of motoneurons of this study are widely distributed (359,000 to 604,000 μm^2), they are slightly biased towards the larger end of the spectrum.

Finally, the motoneurons of this study ranged across three spinal segments (C2-C4) and were collected from three separate animals. These two factors reduce the possibility of location and animal dependent biases.

Taken together, the five cells of this study are representative of a wide range of splenius motoneurons based on their morphological characteristics and location within the spinal cord. Yet, despite the morphological and location differences between these motoneurons, there were strong and consistent trends in the distribution of NE and 5-HT contacts to these motoneurons. The consistency of these patterns indicates that the distribution of NE and 5-HT contacts on splenius motoneurons is independent of their morphological characteristics and location within the spinal cord.

4.1.2 Labeling of Contacts

NE and 5-HT contacts were not assigned with 100% accuracy. Previous studies that have used the same criteria for identifying synapses that we have used for this study, have shown that approximately 90% of the identified contacts are true synapses (Fyffe, 1991; Markam et al. 1997; Alvarez et al. 1998; Lübke et al. 2000; Silver et al. 2003). Undetected gaps between dendrites and boutons, or the presence of thin glial slips existing between dendrites and adjacent boutons (beyond the resolution of a light microscope) result in the mislabeling of contacts (Fyffe, 1991; Alvarez et al. 1998). Therefore, the absolute number of contacts reported in this study is likely an overestimate of the true number of synapses. Additionally, since the same fluorochrome used for labelling dendrites was also used for labelling 5-HT contacts, while NE contacts were labeled with a different fluorochrome, there is the potential that one type of contact was identified with a greater efficacy. However, the focus of this thesis is the distribution of contacts, and not their absolute number and/or densities. There is no evidence for, or reason to believe, that mislabelled contacts would be biased to any particular area. Therefore, while our technique for identifying contacts may affect the absolute number of contacts reported, the trends and patterns detailed in this thesis would not be affected by these issues.

Visibility of 5-HT contacts was obscured in some areas of three motoneurons, due to the intensity of the intracellular staining. This precluded the identification of 5-HT contacts in several small regions (See Results). Of the 44 primary dendrites observed across the five cells, 7 primary dendrites had regions that could not be analyzed for 5-HT

contacts. These regions ranged from 12 to 61 μm from the cell body, which represented only a small proportion of the total dendritic tree (0.5% or less of the total dendritic surface area, for each of the three cells). These regions did not display any unique features with respect to morphology or the labeling of NE contacts, and there were no unique feature with respect to the 5-HT labelling in adjacent areas. Having ruled out these morphological and histological considerations, we have no reason to believe that these small regions of intense intracellular staining would have a novel distribution of 5-HT contacts. The unclear zones were excluded from the analysis of 5-HT contacts along the 7 affected primary dendrites. Therefore, our inability to identify 5-HT contacts on these small regions is unlikely to affect our analyses and our conclusions.

4.1.3 Volume Transmission

Some 5-HT and NE boutons release neurotransmitter extra-synaptically, and can activate extra-synaptic 5-HT receptors. This process is referred to as volume transmission (Beaudet & Descarries, 1978). Volume transmission has been shown in the rat cortex for 5-HT, and NE (Beaudet & Descarries, 1978; Séguéla et al. 2000). There have been no reports of volume transmission within the ventral horn of the spinal cord, and it may be a cortex specific phenomena. The glial in the ventral horn are known to take up extracellular serotonin, strongly limiting the spread of extra-synaptic 5-HT (Fuller & Wong, 1990). In the turtle, 5-HT has been applied to various parts of spinal motoneurons via microiontophoresis through micropipettes (Perrier & Cotel, 2008). This injection method of 5-HT had extremely localized effects within the spinal cord. For instance,

application of 5-HT to the initial segment did not affect somatic 5-HT receptors, and vice versa, suggesting the spread/diffusion of 5-HT is very limited in the ventral horn (Perrier & Cotel, 2008). While it is possible that volume transmission of 5-HT and NE occurs around feline splenius motoneurons, the current literature suggests that neurotransmitter spread would be highly constrained. Whether such a constrained form of volume transmission is sufficient to modulate motoneurons is unknown.

4.1.4 Comparison of Observed Distributions to Diameter Weighted Distributions for Nearest Neighbour Analysis

In this study we compared the distribution of 5-HT and NE contacts to those of computer generated distributions of 5-HT and NE respectively. Typically, computer generated distributions of this kind are generated by dividing the membrane surface area of a cell into compartments the size of a contact and assigning a contact to each compartment. Contacts are chosen from this population using a random selection algorithm. This yields a set of uniformly distributed contacts based on the available surface area. However, since the observed distributions of 5-HT and NE contacts on splenius motoneurons were not uniformly distributed, but varied based on dendritic diameter, a typical computer generated distribution was not sufficiently constrained for a rigorous analysis. To account for the diameter biases of the observed contacts, the random selection algorithm was weighted so that the probability of choosing a contact was based on the diameter of dendrite to which that contact was assigned. This process mimicked the diameter biases of the observed 5-HT and NE contacts respectively (see Results). The computer generated distributions that were diameter-weighted allowed us

to compare the observed distributions of 5-HT and NE to more 'realistic' computer generated distributions.

Comparison of the observed distributions and the computer generated distributions that were diameter-weighted revealed that the observed 5-HT and NE contacts tended to cluster close to one-another compared to the computer generated 5-HT and NE contacts. That is, the probability of observing an NE or 5-HT contact in any given area is dependent on the location of other NE or 5-HT contacts in that area respectively. Therefore, despite the additional constraints of diameter-weighting, the computer generated distributions were not able to account for the distribution biases of the observed contacts.

In addition to a bias of 5-HT and NE contacts towards small diameter dendrites, the contacts were also biased towards distal dendrites. While the computer generated distributions that were diameter-weighted provided a close estimate of the observed distal bias, the extent of the observed distal bias was not fully replicated in the computer generated distribution. This raises the question: could the distal bias of the observed distribution lead to the clustering of pairs of NE or 5-HT, and separation between NE and 5-HT contacts? This is unlikely since the trends of the nearest neighbor analysis were independent of the trends in the distal shift. That is, the trends in the nearest neighbour analysis were identical for each cell regardless of the degree of distal shift between computer generated distributions that were uniform and diameter-weighted.

4.2 Regions Devoid of NE and 5-HT Innervation

Previous work has reported a decreased AHP when NE is present, in feline hind limb motoneurons and rat motoneurons (Fung & Barnes, 1987; Parkis et al. 1995; Martinez-Pena y Valenzuela et al. 2004). In experiments by Fung and Barnes (1987), stimulation of Locus Coeruleus, consisting primarily of NE releasing neurons, decreased the time-course of the action potential AHP in feline hind-limb motoneurons. NE synaptic innervation of the soma and/or initial segment is required for such changes in AHP. We observed no NE contacts on either the soma or initial segments on splenius motoneurons, which may speak to a difference between innervation patterns between feline neck and hind limb motoneurons. There is also the possibility that Fung and Barnes (1987) stimulated non-noradrenergic neurons within locus coeruleus. The feline locus coeruleus contains non-noradrenergic neurons, some of which may have effects on the motoneuron's AHP. For instance neurons containing tyrosine hydroxylase and enkephalin have been shown to be present in the feline locus coeruleus (Charnay et al. 1982). Species differences may also explain why rat AHP is altered following bath application of NE (Parkis et al. 1995; Martinez-Pena y Valenzuela et al. 2004). However, there is also the possibility that extra synaptic NE receptors were activated (see *Volume transmission* above). Bath application of NE has been shown to have effects on persistent Na⁺ channels, which are located somatically, to induce rhythmic firing in rat spinal motoneurons (Harvey et al. 2006b). The lack of observed somatic NE contacts in this thesis suggests that synaptic input of NE would not have this effect on feline splenius

motoneurons. This may be due to species differences, differences between sacral and cervical motoneurons, or the activation of extra synaptic NE receptors.

In summary, although there is published work showing modulation of somatic channels by NE in other motoneurons, NE synaptic input is not expected to affect channels located somatically on feline splenius motoneurons.

NE and 5-HT input lowers the threshold of action potential generation (Dai et al. 2002; Fedirchuk & Dai, 2004; Gilmore & Fedirchuk, 2004). This is likely due to hyperpolarizing the activation voltage for fast Na⁺ channels in the initial segment. Without NE and 5-HT contacts located on the initial segment of feline splenius motoneurons, this effect is not expected from synaptic NE and 5-HT input on feline splenius motoneurons. While many of the studies reporting shifts in action potential generation threshold were performed in rats, Dai and colleagues (2002) demonstrated this shift in feline lumbar motoneurons. This raises the two aforementioned, possible explanations, which are differences in motoneuron type, or activation of extra synaptic receptors, both of which require further investigation to answer.

4.3 Preferential Innervation of Dorsal and Ventral Dendrites

The distributions of NE and 5-HT contacts were widespread throughout the dendritic tree. There were also no regions of the dendritic tree lacking either NE or 5-HT innervation. Therefore, all inputs along the dendritic tree are expected to be amplified by NE and 5-HT synaptic input. However, this does not exclude the possibility of dendritic regions with higher NE contact density than 5-HT contact density, or vice versa. Our

COM analysis shows that along the dorsal/ventral axis of the cell, the observed NE and 5-HT contacts were significantly biased to opposite halves of the dendritic tree. This bias is subtle, with the average difference from the NE and 5-HT COMs being only 47.9 μm along the dorsal/ventral axis (less than the average diameter of the cell bodies). The most comprehensive previous study looking at 5-HT contacts did not note any preferential distribution along dendrites of particular orientations (Alvarez et al. 1998). However, the COM analysis implemented in this thesis is a rather unique and sensitive tool, which may detect differences overlooked in other studies. Synaptic inputs along regions of the dendritic tree with a higher degree of NE or 5-HT innervation would experience a higher degree of amplification when one monoaminergic system is active over the other. Therefore, the distributions of NE and 5-HT along the dorsal/ventral axis may allow for a subtle preferential amplification of some inputs over others.

4.4 Preferential Innervation of Small Diameter and Distal Dendrites

NE and 5-HT contacts were more densely distributed on dendrites with diameters less than 2 μm , compared to larger diameter dendrites. This bias towards small diameter dendrites may serve two purposes: 1) to offset synaptic current loss in these regions, and 2) to reduce the attenuation of synaptic currents as they travel from distal dendrites to the soma.

Synaptic current loss occurs more in small diameter dendrites compared to large diameter dendrites. For a given input of depolarizing current, a small diameter dendrite will experience a larger voltage change than a large diameter dendrite. This large voltage

change decreases the driving potential for depolarizing ions, thus decreasing the amount of current generated by the opening of additional synapses (See introduction, section: **‘Interactions Between Synapses Acting on Ionotropic Receptors’**). Therefore, small diameter dendrites will experience a higher degree of sub-linear interactions between closely activated ionotropic receptors. While NE and 5-HT input would not directly decrease these non-linear interactions, NE and 5-HT input would amplify the net synaptic current, thereby counteracting the effects of the sub-linear interaction.

Currents traveling along small diameter dendrites are attenuated more than currents traveling along large diameter dendrites. This is because small diameter dendrites have a larger cytoplasmic resistance than large diameter dendrites. Current traveling along small diameter dendrites may be preferentially amplified through the activation of NE and 5-HT inputs on small diameter dendrites. This amplification would reduce the attenuation of synaptic inputs on small diameter dendrites, and thus increase their overall influence on somatic membrane potential. Selective amplification of current traveling along small diameter dendrites allows for a set of synapses on small diameter dendrites to be strongly regulated via monoamine input. This regulation would be due to synaptic current generated on small diameter dendrites having little effect on somatic depolarization, unless there is additional NE or 5-HT input.

NE contacts have an increased density along distal dendritic locations. Small diameter dendrites are also often located distally. However the bias to small diameter dendrites did not account for the distal bias. This leads to the question: could the distally biased contacts give rise to the apparent diameter bias? This is unlikely, because the

distribution of 5-HT contacts along two cells was not distally biased, and NE and 5-HT contacts along these cells displayed a strong bias towards small diameter dendrites. The functional implications of increased density of NE contacts along distal dendrites is similar to that of placing NE contacts along small diameter dendrites. Distally generated currents will have to travel a greater distance before affecting the somatic membrane potential. This increased distance increases the amount of current attenuation. Thus, preferential innervation of distal dendrites by NE increases the effect of distal synaptic currents on the soma. 5-HT contacts were not significantly biased distally. This is consistent with the finding that 5-HT contacts are distributed roughly proportional to surface area, with respect to distance from soma (Alvarez et al. 1998).

4.5 Importance of the Relative Proximity between NE and 5-HT contacts

The activation of metabotropic 5-HT_{2a/c} and NE alpha₁ receptors cause intracellular signal cascades as shown in Figure 1.5. These signal cascades lead to the activation of PKC, which modulates local voltage dependent/independent channels. The spread of PKC, or other second messengers which activate PKC through the cytoplasm, creates local zones of modulation near active metabotropic receptors. Some components of the signal cascade spread very short distance. For example, Ca⁺⁺ spreads less than 2 μm before decreasing to baseline levels (Sabatini et al. 2000). Other components of second messenger signal cascades, such as IP3 and ERK, are reported to spread 20 μm, and take 100 ms before declining to baseline levels (Santamaria et al. 2006; Wiegert et al. 2007). These distances were measured along dendrites with diameters of about 1.5 μm.

This allows two synapses, located in close proximity to each other, to have overlapping regions of influence. The functional significance of overlapping regions of influence is particularly important, since the induction of long term potentiation (LTP) at a single synapse can reduce the threshold for induction of LTP in neighbouring synapses, but only if the synapses are within 10 μm of one another (Harvey & Svoboda, 2007). This effect on LTP was later shown to be due to the spread of active Ras (Harvey et al. 2008).

4.5.1 Pairs of NE and of 5-HT Contacts are Located in Close Proximity

The region between pairs of NE contacts, or pairs of 5-HT were measured experimentally as the cytoplasmic volume between the contacts. The average cytoplasmic volume between pairs of NE or 5-HT contacts was 19 μm^3 and 14.5 μm^3 respectively. To give perspective, since volume is a non-intuitive measurement: on a 1.5 μm diameter dendrite, the average distance between pairs of NE or 5-HT contacts would be 2.7 μm and 2.1 μm , respectively. This proximity is well within the distances second messengers have been reported to diffuse (see previous section). These distances between contacts are much smaller than expected if each contact was distributed independently of the other (i.e., our computer generated distributions). Our most conservative computer generated distributions of contacts have a median average volume between pairs of 57.6 μm^3 for NE and 47.1 μm^3 for 5-HT, corresponding to 8.1 μm and 6.7 μm distance along a 1.5 μm dendrite respectively. The close proximity of the pairs of NE or 5-HT contacts is therefore not by chance, but is purposefully distributed. The amount of interaction between second messengers generated at co-activated metabotropic

receptors increases with the relative proximity of receptors. The interaction between pairs of NE or 5-HT contacts would be expected to act cooperatively, similar to the cooperation between locally induced sites of LTP via RAS interaction (Harvey & Svoboda, 2007; Harvey et al. 2008). Cooperation between pairs of NE or 5-HT contacts is due to local concentrations of second messengers reaching the threshold required to exert their effect. At high levels of activation, metabotropic inputs in close proximity would saturate the pool of second messengers at a higher rate. Therefore, the close proximity between pairs of NE or 5-HT contacts is expected to have larger cooperative effects at low levels of activation, and have smaller cooperative effects at high degrees of activation, than if the pairs were located further apart.

4.5.2 NE and 5-HT Contacts are Located Far from One Another

The average volume between the nearest neighbours of NE to 5-HT contacts are larger than would be expected if the contacts were arranged independently from one another. That is, NE contacts tended to avoid regions with 5-HT contacts, and vice versa. The volume between NE and 5-HT contacts was $72.9 \mu\text{m}^3$ and $82.0 \mu\text{m}^3$, taken with either NE or 5-HT as the reference, respectively. This volume corresponds to $10.3 \mu\text{m}$ and $11.6 \mu\text{m}$ distance between contacts along a $1.5 \mu\text{m}$ diameter dendrite. While this distance is still within the $20 \mu\text{m}$ distance for IP3 and ERK diffusion, the degree of interaction between these synapses would be minimized due to the large distance between contacts. This indicates that the larger than expected distances between 5-HT and NE contacts serves to minimize the interactions between NE and 5-HT. Therefore, NE and

5-HT synapses are not strategically arranged to act cooperatively to reach threshold concentrations of second messenger. However, because these systems are arranged in this way, the net effect from the co-activation of both systems may be to reduce the amount of saturation of their shared second messenger systems. Such a strategic arrangement between 5-HT and NE contacts allows for a larger dynamic range of monoamine activity related effects within the dendritic trees of splenius motoneurons.

4.6 Conclusion

This is the first study to systematically compare the relative proximity of inputs from two neuromodulatory systems on a contact to contact basis for any type of neuron. The stark contrast between the relative proximity of certain pairs of contacts over others implies an important functional impact in the way this system is designed. Whether the clustering of neuromodulatory inputs is a feature specific to feline splenius motoneurons, or a key feature of neuromodulatory input to many neuronal types, remains unknown. The impact of having synapses located close versus far from each other may have profound effects on the interactions between multiple coactive second messenger systems. However, the degree to which these interactions control the input to neurons remains unknown, since the mechanisms and effects of second messenger system interactions at this level have only recently come under investigation. Further research into second messenger interactions between multiple coactive G protein receptors will be crucial for understanding the functional consequences of organizing neuromodulatory inputs in clusters. While the effects of clustered neuromodulatory inputs to neurons are

hypothesized above, this study is only the first step towards determining the functional impact of clustered neuromodulatory inputs on motoneuron input-output properties.

References

- Alaburda A & Hounsgaard J (2003). Metabotropic modulation of motoneurons by scratch-like spinal network activity. *J Neurosci.* **23**, 8625-8629.
- Alessandri-Haber N, Alcaraz G, Deleuze C, Jullien F, Manrique C, Couraud F, Crest M, & Giraud P (2002). Molecular determinants of emerging excitability in rat embryonic motoneurons. *J Physiol.* **15**,25-39.
- Alvarez FJ, Pearson JC, Harrington D, Dewey D, Torbeck L, & Fyffe RE (1998) Distribution of 5-hydroxytryptamine-immunoreactive boutons on alpha-motoneurons in the lumbar spinal cord of adult cats. *J Comp Neurol.* **30**,69-83.
- Alvarez FJ & Fyffe RE (2007) The continuing case for the Renshaw cell. *J Physiol.* **584**,31-45.
- Anelli R, Sanelli L, Bennett DJ, & Heckman CJ (2007) Expression of L-type calcium channel alpha(1)-1.2 and alpha(1)-1.3 subunits on rat sacral motoneurons following chronic spinal cord injury. *Neuroscience.* **145**,751-763.
- Aston-Jones G & Cohen JD (2005) Adaptive gain and the role of the locus coeruleus-norepinephrine system in optimal performance. *J Comp Neurol.* **493**,99-110.
- Ballou EW, Smith WB, Anelli R, & Heckman CJ (2006) Measuring dendritic distribution of membrane proteins. *J Neurosci Methods.* **156**,257-266.
- Barrett JN & Crill WE (1974) Influence of dendritic location and membrane properties on the effectiveness of synapses on cat motoneurons. *J Physiol.* **239**,325-345.

Barrett JN & Crill WE (1980). Voltage clamp of cat motoneurone somata: properties of the fast inward current. *J Physiol.* **304**, 231-249.

Bayliss DA, Sirois JE, & Talley EM (2003) The TASK family: two-pore domain background K⁺ channels. *Mol Interv.* **4**,205-219.

Berg AP, Talley EM, Manger JP, & Bayliss DA (2004) Motoneurons express heteromeric TWIK-related acid-sensitive K⁺ (TASK) channels containing TASK-1 (KCNK3) and TASK-3 (KCNK9) subunits. *J Neurosci.* **24**,6693-6702

Brännström T (1993) Quantitative synaptology of functionally different types of cat medial gastrocnemius alpha-motoneurons. *J Comp Neurol.* **330**,439-454

Bras H, Destombes J, Gogan P, & Tyc-Dumont S (1987) The dendrites of single brain-stem motoneurons intracellularly labelled with horseradish peroxidase in the cat. An ultrastructural analysis of the synaptic covering and the microenvironment. *Neuroscience.* **22**,971-981

Blomeley C & Bracci E (2005) Excitatory effects of serotonin on rat striatal cholinergic interneurons. *J Physiol.* **569**,715-21.

Bloomfield SA & Miller RF (1986) A functional organization of ON and OFF pathways in the rabbit retina. *J Neurosci.* **6**,1-13.

Bockaert J, Claeysen S, Bécamel C, Dumuis A, & Marin P (2006) Neuronal 5-HT metabotropic receptors: fine-tuning of their structure, signaling, and roles in synaptic modulation. *Cell Tissue Res.* **326**,553-572.

Brown AG & Fyffe RE (1981) Direct observations on the contacts made between Ia afferent fibres and alpha-motoneurons in the cat's lumbosacral spinal cord. *J Physiol.* **313**,121-140.

Bui TV, Cushing S, Dewey D, Fyffe RE, & Rose PK (2003) Comparison of the morphological and electrotonic properties of Renshaw cells, Ia inhibitory interneurons, and motoneurons in the cat. *J Neurophysiol.* **90**,2900-2918.

Bui TV, Ter-Mikaelian M, Bedrossian D, & Rose PK (2006) Computational estimation of the distribution of L-type Ca(2+) channels in motoneurons based on variable threshold of activation of persistent inward currents. *J Neurophysiol.* **95**,225-241.

Burke RE, Fedina L, & Lundberg A (1971) Spatial synaptic distribution of recurrent and group Ia inhibitory systems in cat spinal motoneurons. *J Physiol.* **214**,305-326.

Burke RE, Dum RP, Fleshman JW, Glenn LL, Lev-Tov A, O'Donovan MJ, & Pinter MJ (1982) A HRP study of the relation between cell size and motor unit type in cat ankle extensor motoneurons. *J Comp Neurol.* **209**,17-28.

Burke RE, Fyffe RE, & Moschovakis AK (1994) Electrotonic architecture of cat gamma motoneurons. *J Neurophysiol.* **72**,2302-2316.

Burke RE & Glenn LL (1996). Horseradish peroxidase study of the spatial and electrotonic distribution of group Ia synapses on type-identified ankle extensor motoneurons in the cat. *J Comp Neurol.* **372**, 465-485.

Burrell BD & Crisp KM (2008) Serotonergic modulation of afterhyperpolarization in a neuron that contributes to learning in the leech. *J Neurophysiol.* **99**, 605-16.

Cameron WE, Averill DB, & Berger AJ (1985) Quantitative analysis of the dendrites of cat phrenic motoneurons stained intracellularly with horseradish peroxidase. *J Comp Neurol.* **231**,91-101

Cameron WE, He F, Kalipatnapu P, Jodkowski JS, & Guthrie RD (1991) Morphometric analysis of phrenic motoneurons in the cat during postnatal development. *J Comp Neurol.* **314**,763-76.

Carlin KP, Jones KE, Jiang Z, Jordan LM, & Brownstone RM (2000) Dendritic L-type calcium currents in mouse spinal motoneurons: implications for bistability. *Eur J Neurosci.* **12**,1635-1646

Carr PA, Pearson JC, & Fyffe RE (1999) Distribution of 5-hydroxytryptamine-immunoreactive boutons on immunohistochemically-identified Renshaw cells in cat and rat lumbar spinal cord. *Brain Res.* **823**,198-201.

Conradi S, Kellerth JO, Berthold CH, & Hammarberg C (1997) Electron microscopic studies of serially sectioned cat spinal alpha-motoneurons. IV. Motoneurons innervating slow-twitch (type S) units of the soleus muscle. *J Comp Neurol.* **184**,769-782.

Crill WE (1996) Persistent sodium current in mammalian central neurons. *Annu Rev Physiol.* **58**,349-362.

Cullheim S, Fleshman JW, Glenn LL, & Burke RE (1987) Membrane area and dendritic structure in type-identified triceps surae alpha motoneurons. *J Comp Neurol.* **255**,68-81.

Cushing S, Bui T, & Rose PK (2005) Effect of nonlinear summation of synaptic currents on the input-output properties of spinal motoneurons. *J Neurophysiol.* **94**,3465-3478.

Delgado-Lezama R, Perrier JF, Nedergaard S, Svirskis G, & Hounsgaard J (1997) Metabotropic synaptic regulation of intrinsic response properties of turtle spinal motoneurons. *J Physiol.* **504**,97-102.

Delgado-Lezama R, Perrier JF & Hounsgaard J (1999). Oscillatory interaction between dorsal root excitability and dorsal root potentials in the spinal cord of the turtle.

Neuroscience. **93**, 731-739.

DiFrancesco D & Borner JS (2007). The funny current: cellular basis for the control of heart rate. *Drugs*. **67** Suppl 2, 15-24

Duman RS (1998) Novel therapeutic approaches beyond the serotonin receptor.

Biol Psychiatry. **44**,324-35.

Elbasiouny SM, Bennett DJ, & Mushahwar VK (2005) Simulation of dendritic CaV1.3 channels in cat lumbar motoneurons: spatial distribution. *J Neurophysiol*. **94**,3961-3674.

Elbasiouny SM, Bennett DJ, & Mushahwar VK (2006) Simulation of Ca²⁺ persistent inward currents in spinal motoneurons: mode of activation and integration of synaptic inputs. *J Physiol*. **570**,355-374.

Fedirchuk B & Dai Y (2004). Monoamines increase the excitability of spinal neurones in the neonatal rat by hyperpolarizing the threshold for action potential production. *J*

Physiol. **557(Pt 2)**,355-361

Fink KB & Göthert M (2007). 5-HT receptor regulation of neurotransmitter release.

Pharmacol Rev. **59**, 360-417.

Franceschetti S, Taverna S, Sancini G, Panzica F, Lombardi R, &Avanzini G (2000)

Protein kinase C-dependent modulation of Na⁺ currents increases the excitability of rat neocortical pyramidal neurones. *J Physiol*. **528**,291-304.

Fukunishi Y, Nagase Y, Yoshida A, Moritani M, Honma S, Hirose Y, & Shigenaga Y (1999) Quantitative analysis of the dendritic architectures of cat hypoglossal motoneurons stained intracellularly with horseradish peroxidase. *J Comp Neurol.* **405**,345-58.

Fung SJ, & Barnes CD (1987) Membrane excitability changes in hindlimb motoneurons induced by stimulation of the locus coeruleus in cats. *Brain Res.* **402**,230-242.

Fyffe RE (1991) Glycine-like immunoreactivity in synaptic boutons of identified inhibitory interneurons in the mammalian spinal cord. *Brain Res.* **547**,175-179

Fyffe RE & Light AR (1984). The ultrastructure of group Ia afferent fiber synapses in the lumbosacral spinal cord of the cat. *Brain Res.* **300**, 201-209.

García-López P, García-Marín V, & Freire M (2006) Three-dimensional reconstruction and quantitative study of a pyramidal cell of a Cajal histological preparation. *J Neurosci.* **26**,11249-11252.

Gilmore J & Fedirchuk FB (2004). The excitability of lumbar motoneurons in the neonatal rat is increased by a hyperpolarization of their voltage threshold for activation by descending serotonergic fibres. *J Physiol.* **558(Pt 1)**, 213-224.

Gladden MH, Maxwell DJ, Sahal A, & Jankowska E (2000) Coupling between serotonergic and noradrenergic neurones and gamma-motoneurons in the cat. *J Physiol.* **527**,213-223.

Grande G, Armstrong S, Neuber-Hess M, & Rose PK (2005) Distribution of contacts from vestibulospinal axons on the dendrites of splenius motoneurons. *J Comp Neurol.* **491**,339-351.

Grande G, Bui TV, & Rose PK (2007a) Estimates of the location of L-type Ca²⁺ channels in motoneurons of different sizes: a computational study. *J Neurophysiol.* **97**,4023-4035.

Grande G, Bui TV, & Rose PK (2007b) Effect of localized innervation of the dendritic trees of feline motoneurons on the amplification of synaptic input: a computational study. *J Physiol.* **583**,611-630.

Granit R, Kernell D, Shortess GK (1963) Quantitative aspects of repetitive firing of mammalian motoneurons, caused by injected currents. *J Physiol.* **168**,911-931.

Granit R, Kernell D, & Lamarre Y (1966) Algebraical summation in synaptic activation of motoneurons firing within the 'primary range' to injected currents. *J Physiol.* **187**,379-399.

Grunnet M, Jespersen T, & Perrier JF (2004) 5-HT_{1A} receptors modulate small-conductance Ca²⁺-activated K⁺ channels. *J Neurosci Res.* **78**,845-854.

Guertin PA, & Hounsgaard J (1999) L-type calcium channels but not N-methyl-D-aspartate receptor channels mediate rhythmic activity induced by cholinergic agonist in motoneurons from turtle spinal cord slices. *Neurosci Lett.* **261**,81-84.

Hammar I, Bannatyne BA, Maxwell DJ, Edgley SA, & Jankowska E (2004) The actions of monoamines and distribution of noradrenergic and serotonergic contacts on different subpopulations of commissural interneurons in the cat spinal cord. *Eur J Neurosci.* **19**,1305-1316.

Hammar I & Maxwell DJ (2002). Serotonergic and noradrenergic axons make contacts with neurons of the ventral spinocerebellar tract in the cat. *J Comp Neurol.* **443**, 310-319

Harvey PJ, Li X, Li Y, & Bennett DJ (2006a) Endogenous monoamine receptor activation is essential for enabling persistent sodium currents and repetitive firing in rat spinal motoneurons. *J Neurophysiol.* **96**,1171-1186.

Harvey PJ, Li Y, Li X, & Bennett DJ (2006b) Persistent sodium currents and repetitive firing in motoneurons of the sacrocaudal spinal cord of adult rats. *J Neurophysiol.* **96**,1141-1157.

Harvey PJ, Li X, Li Y, & Bennett DJ (2006c) 5-HT₂ receptor activation facilitates a persistent sodium current and repetitive firing in spinal motoneurons of rats with and without chronic spinal cord injury. *J Neurophysiol.* **96**,1158-1170.

Harvey CD & Svoboda K (2007). Locally dynamic synaptic learning rules in pyramidal neuron dendrites. *Nature.* **450**, 1195-1200.

Harvey CD, Yasuda R, Zhong H, & Svoboda K (2008) The spread of Ras activity triggered by activation of a single dendritic spine. *Science.* 321,136-140.

Hayar A, Heyward PM, Heinbockel T, Shipley MT, & Ennis M (2001) Direct excitation of mitral cells via activation of alpha1-noradrenergic receptors in rat olfactory bulb slices. *J Neurophysiol.* **86**,2173-2182.

Heckman CJ, Kuo JJ, & Johnson MD (2004) Synaptic integration in motoneurons with hyper-excitable dendrites. *Can J Physiol Pharmacol.* **82**,549-55.

Heckman CJ, Lee RH, & Brownstone RM (2003) Hyperexcitable dendrites in motoneurons and their neuromodulatory control during motor behavior. *Trends Neurosci.* **26**,688-695.

Heckman CJ, Johnson M, Mottram C, & Schuster J (2008) Persistent inward currents in spinal motoneurons and their influence on human motoneuron firing patterns. *Neuroscientist.* **14**,264-275.

Hornby TG, McDonagh JC, Reinking RM, & Stuart DG (2002) Effects of excitatory modulation on intrinsic properties of turtle motoneurons. *J Neurophysiol.* **88**,86-97.

Hounsgaard J, Hultborn H, Jespersen B, & Kiehn O (1984) Intrinsic membrane properties causing a bistable behaviour of alpha-motoneurons. *Exp Brain Res.* **55**,391-394.

Hounsgaard J, Hultborn H, Jespersen B, & Kiehn O (1988) Bistability of alpha-motoneurons in the decerebrate cat and in the acute spinal cat after intravenous 5-hydroxytryptophan. *J Physiol.* 1988 Nov;405:345-67.

Hounsgaard J & Kiehn O (1985). Ca⁺⁺ dependent bistability induced by serotonin in spinal motoneurons. *Exp Brain Res.* **57**, 422-425.

Hounsgaard J & Kiehn O (1989). Serotonin-induced bistability of turtle motoneurons caused by a nifedipine-sensitive calcium plateau potential. *J Physiol.* **414**, 265-282.

Hsiao CF, Trueblood PR, Levine MS, & Chandler SH (1997) Multiple effects of serotonin on membrane properties of trigeminal motoneurons in vitro. *J Neurophysiol.* **77**,2910-2924.

Hsiao CF, Del Negro CA, Trueblood PR, & Chandler SH (1998) Ionic basis for serotonin-induced bistable membrane properties in guinea pig trigeminal motoneurons. *J Neurophysiol.* **79**,2847-2856.

Hultborn H, Denton ME, Wienecke J, & Nielsen JB (2003) Variable amplification of synaptic input to cat spinal motoneurons by dendritic persistent inward current. *J Physiol.* **552**,945-52.

Hynstrom AS, Johnson MD, Miller JF, & Heckman CJ (2007) Intrinsic electrical properties of spinal motoneurons vary with joint angle. *Nat Neurosci.* **10**,363-369.

Jiao Y, Sun Z, Lee T, Fusco FR, Kimble TD, Meade CA, Cuthbertson S, & Reiner A (1999) A simple and sensitive antigen retrieval method for free-floating and slide-mounted tissue sections. *J Neurosci Methods.* **15**,149-162.

Jones SM & Lee RH (2006) Fast amplification of dynamic synaptic inputs in spinal motoneurons in vivo. *J Neurophysiol.* **96**:2200-2206.

Jordan LM, Liu J, Hedlund PB, Akay T, & Pearson KG (2008) Descending command systems for the initiation of locomotion in mammals. *Brain Res Rev.* **57**,183-91.

Kiehn O & Harris-Warrick RM (1992) 5-HT modulation of hyperpolarization-activated inward current and calcium-dependent outward current in a crustacean motor neuron. *J Neurophysiol.* **68**,496-508.

Keirstead SA & Rose PK (1983) Dendritic distribution of splenius motoneurons in the cat: comparison of motoneurons innervating different regions of the muscle. *J Comp Neurol.* **219**, 273-84.

Kernell D & Zwaagstra B (1989a) Dendrites of cat's spinal motoneurons: relationship between stem diameter and predicted input conductance. *J Physiol.* **413**, 255-69.

Kernell D & Zwaagstra B (1989b) Size and remoteness: two relatively independent parameters of dendrites, as studied for spinal motoneurons of the cat. *J Physiol.* **413**, 233-54.

Koch C, Poggio T & Torre V (1983) Nonlinear interactions in a dendritic tree: localization, timing and role in information processing. *Proc Natl Acad Sci* **80**, 2799-2802.

Koch C (1984) Cable theory in neurons with active, linearized membranes. *Biol Cybern.* **50**,15-33.

Koizumi & Smith (2008) Persistent Na⁺ and K⁺-dominated leak currents contribute to respiratory rhythm generation in the pre-Bötzinger complex in vitro. *J Neurosci.* **28**, 1773-1785.

Korogod SM, Kulagina IB, Horcholle-Bossavit G, Gogan P, & Tyc-Dumont S (2000) Activity-dependent reconfiguration of the effective dendritic field of motoneurons. *J Comp Neurol.* **422**,18-34.

Korkotian E & Segal M (2006) Spatially confined diffusion of calcium in dendrites of hippocampal neurons revealed by flash photolysis of caged calcium. *Cell Calcium.* **40**, 441-449.

Koschak A, Reimer D, Walter D, Hoda JC, Heinzle T, Grabner M, & Striessnig J (2003) Cav1.4alpha1 subunits can form slowly inactivating dihydropyridine-sensitive L-type Ca²⁺ channels lacking Ca²⁺-dependent inactivation. *J Neurosci.* **23**,6041-6049.

Lee RH, Kuo JJ, Jiang MC, & Heckman CJ (2003) Influence of active dendritic currents on input-output processing in spinal motoneurons in vivo. *J Neurophysiol.* **89**,27-39.

Lee RH & Heckman CJ (1996). Influence of voltage-sensitive dendritic conductances on bistable firing and effective synaptic current in cat spinal motoneurons in vivo. *J Neurophysiol.* **76**, 2107-2110.

Lee RH & Heckman CJ (1998a) Bistability in spinal motoneurons in vivo: systematic variations in persistent inward currents. *J Neurophysiol.* **80**, 583-593.

Lee RH & Heckman CJ (1998b) Bistability in spinal motoneurons in vivo: systematic variations in rhythmic firing patterns. *J Neurophysiol.* **80**, 572-582.

Lee RH, & Heckman CJ (1999) Enhancement of bistability in spinal motoneurons in vivo by the noradrenergic alpha1 agonist methoxamine. *J Neurophysiol.* **81**,2164-2174.

Lee RH & Heckman CJ (2000). Adjustable amplification of synaptic input in the dendrites of spinal motoneurons in vivo. *J Neurosci.* **20**, 6734-6740.

Lee RH & Heckman CJ (2001). Essential role of a fast persistent inward current in action potential initiation and control of rhythmic firing. *J Neurophysiol.* **85**, 472-475.

Li Y, Gorassini MA, & Bennett DJ (2004) Role of persistent sodium and calcium currents in motoneuron firing and spasticity in chronic spinal rats. *J Neurophysiol.* **91**,767-783.

Li Y & Bennett DJ (2003). Persistent sodium and calcium currents cause plateau potentials in motoneurons of chronic spinal rats. *J Neurophysiol.* **90**, 857-869.

Lodish H, Berk A, Zipursky S.L., Matsudaira P, Baltimore D & Darnell J (2000) Cell-to-cell signaling: Hormones and Receptors. In: *Molecular cell biology, 4th ED*. Edited by Tenney S: W.H. Freeman and Company

Lörincz A, Notomi T, Tamás G, Shigemoto R, & Nusser Z (2002) Polarized and compartment-dependent distribution of HCN1 in pyramidal cell dendrites. *Nat Neurosci.* **5**,1185-1193.

Lübke J, Egger V, Sakmann B, & Feldmeyer D (2000) Columnar organization of dendrites and axons of single and synaptically coupled excitatory spiny neurons in layer 4 of the rat barrel cortex. *J Neurosci.* **20**,5300-5311.

Magee JC (1999) Dendritic Ih normalizes temporal summation in hippocampal CA1 neurons. *Nat Neurosci.* **2**,848.

Manuel M, Meunier C, Donnet M, & Zytnicki D (2006) The afterhyperpolarization conductance exerts the same control over the gain and variability of motoneurone firing in anaesthetized cats. *J Physiol.* **576**,873-886.

Maronde E, Schomerus C, Stehle JH, & Korf HW (1997) Control of CREB phosphorylation and its role for induction of melatonin synthesis in rat pinealocytes. *Biol Cell.* **89**,505-511.

Matsumoto M & Yoshioka M (2001). [Intracellular signal transduction mediated via 5-HT and NA receptors]. *Nippon Rinsho.* **59**,1450-1456.

McCamphill PK, Dunn TW, & Syed NI (2008) Serotonin modulates transmitter release at central *Lymnaea* synapses through a G-protein-coupled and cAMP-mediated pathway. *Eur J Neurosci.* **27**,2033-2042.

Michelotti GA, Price DT, & Schwinn DA (2000) Alpha 1-adrenergic receptor regulation: basic science and clinical implications. *Pharmacol Ther.* **88**,281-309.

Migliore M & Shepherd GM (2002). Emerging rules for the distributions of active dendritic conductances. *Nat Rev Neurosci.* **3**, 362-370.

Miles GB, Hartley R, Todd AJ, & Brownstone RM (2007) Spinal cholinergic interneurons regulate the excitability of motoneurons during locomotion. *Proc Natl Acad Sci U S A.* **104**,2448-2453.

Milligan CJ, Edwards IJ, & Deuchars J (2006) HCN1 ion channel immunoreactivity in spinal cord and medulla oblongata. *Brain Res.* **1081**,79-91.

Moritani M, Kida H, Nagase Y, Fukami H, Honma S, Takemura M, Masuda Y, Bae YC, Shigenaga Y, & Yoshida A (2003) Quantitative analysis of the dendritic architectures of single jaw-closing and jaw-opening motoneurons in cats. *Exp Brain Res.* **150**,265-275.

Moritz AT, Newkirk G, Powers RK, & Binder MD (2007) Facilitation of somatic calcium channels can evoke prolonged tail currents in rat hypoglossal motoneurons. *J Neurophysiol.* **98**,1042-1047.

Nagase Y, Moritani M, Nakagawa S, Yoshida A, Takemura M, Zhang LF, Kida H, & Shigenaga Y (1997) Serotonergic axonal contacts on identified cat trigeminal

motoneurons and their correlation with medullary raphe nucleus stimulation. *J Comp Neurol.* **384**,443-445.

Núñez-Abades PA, He F, Barrionuevo G, & Cameron WE (1994) Morphology of developing rat genioglossal motoneurons studied in vitro: changes in length, branching pattern, and spatial distribution of dendrites. *J Comp Neurol.* **339**,401-420.

Parkis MA, Bayliss DA, & Berger AJ (1995) Actions of norepinephrine on rat hypoglossal motoneurons. *J Neurophysiol.* **74**,1911-1919

Perrier JF, Alaburda A, & Hounsgaard J (2002) Spinal plasticity mediated by postsynaptic L-type Ca²⁺ channels. *Brain Res Rev.* **40**,223-229.

Perrier JF, Alaburda A, & Hounsgaard J (2003) 5-HT_{1A} receptors increase excitability of spinal motoneurons by inhibiting a TASK-1-like K⁺ current in the adult turtle. *J Physiol.* **548**,485-492.

Perrier JF & Hounsgaard J (2003). 5-HT₂ receptors promote plateau potentials in turtle spinal motoneurons by facilitating an L-type calcium current. *J Neurophysiol.* **89**, 954-959.

Powers RK, & Binder MD (2001) Input-output functions of mammalian motoneurons. *Rev Physiol Biochem Pharmacol.* **143**,137-263.

Prather JF, Powers RK, & Cope TC (2001) Amplification and linear summation of synaptic effects on motoneuron firing rate. *J Neurophysiol.* **85**,43-53.

Rall W, Burke RE, Smith TG, Nelson PG, & Frank K (1967) Dendritic location of synapses and possible mechanisms for the monosynaptic EPSP in motoneurons. *J Neurophysiol.* **30**,1169-1193.

Rall W (1977). Core conductor theory and cable properties of neurons. In: *Handbook of Physiology. The nervous System, vol I. Cellular biology of neurons. Part I.* edited by Kandel ER. Bethesda, MD: American Physiological Society

Rank MM, Li X, Bennett DJ, & Gorassini MA (2007) Role of endogenous release of norepinephrine in muscle spasms after chronic spinal cord injury. *J Neurophysiol.* **97**,3166-3180.

Rekling JC, Funk GD, Bayliss DA, Dong XW, & Feldman JL (2000) Synaptic control of motoneuronal excitability. *Physiol Rev.* **80**,767-852.

Rose PK (1981) Distribution of dendrites from biventer cervicis and complexus motoneurons stained intracellularly with horseradish peroxidase in the adult cat. *J Comp Neurol.* **197**, 395-409.

Rose PK, Keirstead SA, Vanner SJ (1985). A quantitative analysis of the geometry of cat motoneurons innervating neck and shoulder muscles. *J Comp Neurol.* **239**, 89-107.

Rose PK, MacDonald J, Abrahams VS (1991). Projections of the tectospinal tract to the upper cervical spinal cord of the cat: a study with the anterograde tracer PHA-L. *J Comp Neurol.* **314**, 91-105.

Rose PK, Jones T, Nirula R, & Corneil T (1995). Innervation of motoneurons based on dendritic orientation. *J Neurophysiol.* **73**, 1319-22.

Rose PK & Cushing S (1999). Non-linear summation of synaptic currents on spinal motoneurons: lessons from simulations of the behaviour of anatomically realistic models. *Prog Brain Res.* **123**, 99-107.

Rose PK & Cushing S (2004). Relationship between morphoelectrotonic properties of motoneuron dendrites and their trajectory. *J Comp Neurol.* **473**, 562-581.

Rose PK & Neuber-Hess M (1991). Morphology and frequency of axon terminals on the somata, proximal dendrites, and distal dendrites of dorsal neck motoneurons in the cat. *J Comp Neurol.* **307**, 259-280.

Sabatini BL, Maravall M, & Svoboda K (2001) Ca(2+) signaling in dendritic spines. *Curr Opin Neurobiol.* **11**,349-356.

Santamaria F, Wils S, De Schutter E, & Augustine GJ (2006) Anomalous diffusion in Purkinje cell dendrites caused by spines. *Neuron.* **22**,635-634.

Schwandt PC, & Calvin WH (1973) Equivalence of synaptic and injected current in determining the membrane potential trajectory during motoneuron rhythmic firing. *Brain Res.* **14**,389-94.

Schwandt P & Crill WE (1977). A persistent negative resistance in cat lumbar motoneurons. *Brain Res.* **120**, 173-178.

Schwandt PC, & Crill WE (1980) Properties of a persistent inward current in normal and TEA-injected motoneurons. *J Neurophysiol.* **43**,1700-1724.

Segev I (1998) Sound grounds for computing dendrites. *Nature.* **393**,207-208.

Segev I & Parnas I (1983). Synaptic integration mechanisms. Theoretical and experimental investigation of temporal postsynaptic interactions between excitatory and inhibitory inputs. *Biophys J.* **41**, 41-50

Shapiro NP, Lee RH (2007) Synaptic amplification versus bistability in motoneuron dendritic processing: a top-down modeling approach. *J Neurophysiol.* **97**,3948-3960.

Sherrington CS (1906). *The Integrative Actions of the Nervous System.* New York: Charles Scribner's Sons.

Silver RA, Lubke J, Sakmann B, & Feldmeyer D (2003) High-probability unquantal transmission at excitatory synapses in barrel cortex. *Science.* **12**,1981-1984.

Simon M, Perrier JF, Hounsgaard J (2003) Subcellular distribution of L-type Ca²⁺ channels responsible for plateau potentials in motoneurons from the lumbar spinal cord of the turtle. *Eur J Neurosci.* **18**,258-266.

Sirois JE, Lynch C 3rd, & Bayliss DA (2002). Convergent and reciprocal modulation of a leak K⁺ current and I(h) by an inhalational anaesthetic and neurotransmitters in rat brainstem motoneurons. *J. Physiol.* **541**, 717-729

Sun QJ, Berkowitz RG, Goodchild AK, & Pilowsky PM (2002) Serotonin inputs to inspiratory laryngeal motoneurons in the rat. *J Comp Neurol.* **451**,91-98.

Svirskis G & Hounsgaard J (1998). Transmitter regulation of plateau properties in turtle motoneurons. *J Neurophysiol.* **79**, 45-50.

Talley EM, Sadr NN, & Bayliss DA (1997). Postnatal development of serotonergic innervation, 5-HT_{1A} receptor expression, and 5-HT responses in rat motoneurons. *J Neurosci.* **17**, 4473-4485.

Talley EM, & Bayliss DA (2000). TASK-1, a two-pore domain K⁺ channel, is modulated by multiple neurotransmitters in motoneurons. *Neuron.* **25**, 399-410.

Ulfhake B, & Cullheim S (1988) Postnatal development of cat hind limb motoneurons. III: Changes in size of motoneurons supplying the triceps surae muscle. *J Comp Neurol.* **278**,103-120.

Ulfhake B & Kellerth JO (1981). A quantitative light microscopic study of the dendrites of cat spinal alpha-motoneurons after intracellular staining with horseradish peroxidase. *J Comp Neurol.* **202**, 571-83.

Ulfhake B & Kellerth JO (1984). Electrophysiological and morphological measurements in cat gastrocnemius and soleus alpha-motoneurons. *Brain Res.* **307**, 167-179

Martinez-Pena y Valenzuela I, Rogers RC, Hermann GE, & Travagli RA (2004) Norepinephrine effects on identified neurons of the rat dorsal motor nucleus of the vagus. *Am J Physiol Gastrointest Liver Physiol.* **286**,G333-9.

Vanner SJ, Rose PK (1984) Dendritic distribution of motoneurons innervating the three heads of the trapezius muscle in the cat. *J Comp Neurol.* **226**,96-110.

Vetter P, Roth A, & Häusser M (2001) Propagation of action potentials in dendrites depends on dendritic morphology. *J Neurophysiol.* **85**,926-937.

Wallén P, Buchanan JT, Grillner S, Hill RH, Christenson J, & Hökfelt T (1989) Effects of 5-hydroxytryptamine on the afterhyperpolarization, spike frequency regulation, and oscillatory membrane properties in lamprey spinal cord neurons. *J Neurophysiol.* **61**,759-768.

Wallén P, Christenson J, Brodin L, Hill R, Lansner A, & Grillner S (1989) Mechanisms underlying the serotonergic modulation of the spinal circuitry for locomotion in lamprey. *Prog Brain Res.* **80**,315-327.

Westenbroek RE, Hoskins L, & Catterall WA (1998) Localization of Ca²⁺ channel subtypes on rat spinal motor neurons, interneurons, and nerve terminals. *J Neurosci.* **18**,6319-6330.

Wiegert JS, Bengtson CP, & Bading H (2007) Diffusion and not active transport underlies and limits ERK1/2 synapse-to-nucleus signaling in hippocampal neurons. *J Biol Chem.* **282**,29621-29633.

Yabuta NH, Yasuda K, Nagase Y, Yoshida A, Fukunishi Y, & Shigenaga Y (1996) Light microscopic observations of the contacts made between two spindle afferent types and alpha-motoneurons in the cat trigeminal motor nucleus. *J Comp Neurol.* **374**,436-450.

Yates BJ, Goto T, Kerman I, & Bolton PS (1993) Responses of caudal medullary raphe neurons to natural vestibular stimulation. *J Neurophysiol.* **70**,938-946.